Retrieving robust noise-based seismic velocity changes from sparse data sets: synthetic tests and application to Klyuchevskoy volcanic group (Kamchatka)

C Gómez-García, F. Brenguier, P. Boue, N. M. Shapiro, D V Droznin, S. Ya. Droznina, S. L. Senyukov, E. I. Gordeev

Retrieving robust noise-based seismic velocity changes from sparse data sets: synthetic tests and application to Klyuchevskoy volcanic group (Kamchatka)

C Gómez-García, F. Brenguier, P. Boue, N. M. Shapiro, D Droznin, S Ya Droznina, S. L. Senyukov, E. I. Gordeev

submitted to *Geophys. J. Int.*

Retrieving robust noise-based seismic velocity changes from sparse data sets: synthetic tests and application to Klyuchevskoy volcanic group (Kamchatka)

C. Gómez-García[1,6], F. Brenguier[2], P. Boué[2], N.M. Shapiro[3,4], D.V. Droznin[5], S. Ya. Droznina[5], S.L. Senyukov[5] and E.I. Gordeev[4]

[1]*Instituto de Ciencias de la Tierra Jaume Almera, CSIC, Lluís Solé i Sabarís s/n, E-08028 Barcelona, Spain*

[2]*Institut des Sciences de la Terre, Université Grenoble Alpes, F-38041 Grenoble cedex 9, France*

[3]*Institut de Physique du Globe de Paris, Paris Sorbonne Cité, CNRS, 1 rue Jussieu, F-75238 Paris cedex 05, France*

[4]*Institute of Volcanology and Seismology FEB RAS, 9 Piip Boulevard, Petropavlovsk-Kamchatsky, Kamchatsky Region 683006, Russia*

[5]*Kamchatka Branch of the Geophysical Service, Russian Academy of Sciences, 9 Piip Boulevard, Petropavlovsk-Kamchatsky, Kamchatsky Region 683006, Russia*

[6]Now at *Dublin Institute for Advanced Studies, Geophysics Section, 5 Merrion Square, Dublin 2, Ireland*

E-mail: cgomez@cp.dias.ie

SUMMARY

Continuous noise-based monitoring of seismic velocity changes provides insights into volcanic unrest, earthquake mechanisms and fluid injection in the sub-surface. The standard monitoring approach relies on measuring travel time changes of late coda arrivals between daily and reference noise-cross-correlations, usually chosen as stacks of daily cross-correlations. The main assumption of this method is that the shape of the noise correlations does not change over time or, in other terms, that the ambient-noise sources are stationary through time. These conditions are not fulfilled when a strong episodic source of noise, such as volcanic tremor, for example, perturbs the reconstructed Green's function. In this paper we propose a general formulation for retrieving continuous time series of noise-based seismic velocity changes without the requirement of any arbitrary reference cross-correlation function. We perform synthetic tests in order to establish a general framework for future applications of this technique. In particular, we study the reliability of velocity changes measurements versus the stability of noise cross-correlation functions. We apply this approach to a complex dataset of noise cross-correlations at Klyuchevskoy volcanic group (Kamchatka), hampered by loss of data and the presence of highly non-stationary seismic tremor.

Key words: Seismic noise; Time series analysis; Volcano monitoring; Seismic interferometry; Coda waves.

1 INTRODUCTION

Noise-based monitoring techniques have been used extensively in the past decade for different applications. The observation of continuous seismic velocity changes proved to be useful for detecting crustal seasonal changes (e.g., Sens-Schönfelder & Wegler 2006; Meier et al. 2010; Ugalde et al. 2014), co- and post-seismic evolution of stress in fault areas (e.g., Brenguier et al. 2008a; Hobiger et al. 2012) and, more recently, for stuying the effects of fluid injection (e.g., Zhou et al. 2010; Ugalde et al. 2013) and aseismic deformation transients (Hillers et al. 2015).

Estimation of temporal velocity changes in volcano interiors using seismic noise cross-correlation has been shown to be an efficient method for early detection of volcanic unrest prior to eruptions at Piton de la Fournaise Volcano, La Réunion (e.g., Brenguier et al. 2008b; Duputel et al. 2009). Although precise eruption and eruption intensity forecasting is still a challenge, it has been demonstrated that this method provides meaningful constraints on the location of oncoming eruptions (Obermann et al. 2013).

The most important step in noise-based monitoring is the reconstruction of Green's function (GF) between two receivers from the correlation of ambient seismic noise (e.g., Shapiro & Campillo 2004; Shapiro et al. 2005; Larose et al. 2006; Wapenaar et al. 2010; Campillo et al. 2011). If the noise sources are evenly distributed over the Earth's surface, leading to an isotropic and equipartioned wavefield at the two station locations, the cross-correlation function (CCF) between these two stations converges towards the GF (e.g., Roux et al. 2005; Wapenaar & Fokkema 2006). This is an ideal situation but, in practice, noise sources are distributed irregularly leading to a partial reconstruction of the GF (Shapiro et al. 2006).

For monitoring purposes, it is possible to retrieve temporal seismic velocity changes over a set of repetitive in time noise cross-correlations, even with anisotropic distributions of noise sources, as long as this distribution does not change too much over time (Hadziioannou et al. 2009). Moreover, measuring travel time changes in the coda part of the noise cross-correlations makes velocity change measurements less sensitive to noise source temporal changes (Sens-Schönfelder & Wegler 2006; Wegler & Sens-Schönfelder 2007; Colombi et al. 2014). The standard monitoring approach relies on measuring travel time changes of late coda arrivals between a daily and a reference noise-cross-correlation, usually chosen as a stack of all daily cross-correlations. We assume that the measured time delay from the coda waveform of noise cross-correlations ($d\tau$) is caused by a spatially homogeneous relative velocity change, $d\nu/\nu$. Under this assumption, the relative delay time ($d\tau/\tau$) is constant and independent of the lapse time at which it is measured: $d\tau/\tau = -d\nu/\nu$.

In different environments, and especially on volcanoes, the noise correlations can be altered by strong episodic sources of noise as volcanic tremor, for example, that overlaps in frequency with more stable microseismic noise. There is thus a problem with the definition of the reference function if the sources are non-stationary (Sens-Schönfelder et al. 2014). Very strong non-stationary noise has been described by Ballmer et al. (2013) and Droznin et al. (2015) in case of emission of low frequency volcanic tremor, a typical feature of the unrest of many volcanoes and an important seismic source for monitoring plumbing systems (e.g., Chouet 1996).

In this article, we describe a new generalized approach for retrieving continuous time series of noise-based seismic velocity changes without the definition of an arbitrary reference CCF. Brenguier et al. (2014) proposed the method used in this paper (Section 2). We detail the method carrying out synthetic tests that allow us to evaluate the reliability of measured velocity changes in regard to the level of stability of noise cross-correlation functions and the influence of temporary strong changes (Section 3). Finally, we apply our procedure to a real dataset in Section 4. We choose the Klyuchevskoy volcanic group (Kamchatka) as a case study where the recorded wavefield is dominated by strongly localized volcanic tremor sources and is hampered by lose of data and the presence of highly non-stationary seismic noise. This approach will be useful for improving noise-based seismic monitoring at all scales in cases where noise sources are not stable in time.

2 METHOD

The standard approach for measuring continuous time series of noise-based seismic velocity changes relies on measuring travel time differences between a set of noise cross-correlations at different dates and a so-called reference cross-correlation. The reference CCF is usually defined as the stack of all cross-correlations for a given station pair at different days (Brenguier et al. 2008b). Temporal changes of seismic velocities are then measured using a Moving Window Cross Spectral (MWCS) procedure between the daily and reference cross-correlation functions by measuring travel time changes along the coda part of the cross-correlation functions (Clarke et al. 2011).

Here, we propose a general formulation for retrieving continuous time series of velocity changes without the requirement of a reference stacked cross-correlation function. The novel procedure relies on measuring seismic velocity changes between all possible pairs of daily cross-correlation functions. An inversion step is further required to retrieve a continuous time series of daily seismic velocity changes (Brenguier et al. 2014).

By considering (ccf_i) as a cross-correlation function that corresponds to day *i*, we can thus estimate a seismic velocity (ν_{ij}) change between day *i* and day *j* by applying the MWCS analysis to ccf_i and ccf_j:

$$\delta\nu_{ij} = \frac{\nu_j - \nu_i}{\nu_i} = \text{MWCS}(ccf_i, ccf_j) \tag{1}$$

$\delta\nu_{ij}$ is referred as a doublet measurement. This concept was used, initially, in pairs of microearthquakes (Poupinet et al. 1984). In a systematic manner, we can then estimate a velocity change between all of the pairs of daily cross-correlation functions for one given station pair. This constitutes the data vector of Equation (2):

$$\mathbf{d} = \begin{bmatrix} \delta\nu_{12} \\ \delta\nu_{13} \\ \delta\nu_{14} \\ \vdots \\ \delta\nu_{n-1n} \end{bmatrix} \tag{2}$$

where **d** is of length $\frac{n\cdot(n-1)}{2}$, with *n* the number of daily cross-correlation functions.

Our final goal is to reconstruct the time series of daily velocity changes. We can define these velocity changes as $\delta\nu_i = \frac{\nu_i - \nu_{ref}}{\nu_{ref}}$, with ν_{ref} the reference velocity averaged along the entire studied time period. The series of velocity changes constitutes our model vector, **m**, of Equation (3):

$$\mathbf{m} = \begin{bmatrix} \delta\nu_1 \\ \delta\nu_2 \\ \delta\nu_3 \\ \vdots \\ \delta\nu_n \end{bmatrix} \tag{3}$$

where **m** is of length *n*, the number of daily cross-correlation functions.

The relation between **d** and **m** is given by:

$$\delta\nu_j - \delta\nu_i = \frac{\nu_j - \nu_i}{\nu_{ref}} = \frac{\nu_j - \nu_i}{\nu_i} \cdot \frac{\nu_i}{\nu_{ref}} = \delta\nu_{ij} \cdot \frac{\nu_i}{\nu_{ref}} = \delta\nu_{ij} \cdot (1 + \delta\nu_i) \tag{4}$$

Under the assumption that $\delta\nu_i$ and $\delta\nu_{ij}$ are small compared to 1 ($<$ 0.1 %), we can write at the first order the direct linear relationship between **d** and **m** as $\delta\nu_{ij} = \delta\nu_j - \delta\nu_i$ or $\mathbf{d} = \mathbf{G}\mathbf{m}$, with $\mathbf{G}$ being a sparse matrix of dimension $\left[\frac{n\cdot(n-1)}{2}, n\right]$:

$$\mathbf{G} = \begin{bmatrix} -1 & 1 & 0 & \dots & & & \dots & 0 \\ -1 & 0 & 1 & 0 & \dots & & & \vdots \\ -1 & 0 & 0 & 1 & 0 & \dots & & \\ \vdots & & & & & \ddots & & \vdots \\ 0 & \dots & & & & \dots & 0 & -1 & 1 \end{bmatrix} \tag{5}$$

The assumption made above ($\delta\nu_i$ and $\delta\nu_{ij} < 0.1$ %) is necessary to apply our method. Temporal velocity changes ($\delta\nu_i$) are sensitive to transient stress changes (e.g., Niu et al. 2008) and the magnitude order of the seismic velocity changes depends on the level of applied stress in the medium. Some examples of typical magnitude orders of $\delta\nu_i$ estimations are $\sim -0.1\%$ in the Piton de la Fournaise volcano (Brenguier et al. 2008b; Obermann et al. 2013), $\sim -0.12\%$ due to the Tohoku-Oki earthquake (Brenguier et al. 2014), $\sim -0.15\%$ due to the Parkfield earthquake (Schaff 2012), $\sim -0.5\%$ due to the Nicoya Peninsula earthquake (Chaves & Schwartz 2016) or $\sim -0.8\%$ in Ruapehu volcano (Mordret et al. 2010).

The final time series of velocity changes (**m**) is obtained by further inversion, using a classical Bayesian linear least square formulation (Tarantola 2005; details in Brenguier et al. 2014):

$$\mathbf{m} = \left(\mathbf{G}^t\mathbf{C}_\mathbf{d}^{-1}\mathbf{G} + \alpha\mathbf{C}_\mathbf{m}^{-1}\right)^{-1}\mathbf{G}^t\mathbf{C}_\mathbf{d}^{-1}\mathbf{d} \tag{6}$$

where $\mathbf{C}_\mathbf{d}$ is a covariance matrix of dimension $\left[\frac{n\cdot(n-1)}{2}, \frac{n\cdot(n-1)}{2}\right]$ that describes the Gaussian uncertainties of the data vector **d**. These values correspond to the estimated uncertainties of each $\delta\nu_{ij}$ estimate, using the MWCS analysis.

$\mathbf{C_m}$ is an a priori covariance matrix of dimension $[n, n]$ for model vector **m**. The parameter α is a weighting coefficient. It is determined in a way that matrix $\left(\mathbf{G}^t\mathbf{C_d}^{-1}\mathbf{G}\right)$ and $\left(\alpha\mathbf{C_m}^{-1}\right)$ have approximately the same weight. Since α behaves as the amplitude of the inverse of the distribution $\mathbf{C_m}$, the larger the α, the less the model can change from one point to another point and, therefore, the lower the amplitude and smoother the final time series will be.

The values of $\mathbf{C_m}$ describe for day *i* how $\delta\nu_i$ is correlated to $\delta\nu_j$ at day *j*:

$$C_{m_{ij}} = e^{\frac{-|i-j|}{2\beta}} \tag{7}$$

where β is the characteristic correlation length between the model parameters $\delta\nu$. A day, *i*, is more correlated with the β days before and after than with any others. For this reason, large values of β correspond to velocity change curves (long-term variations) that avoid short-term fluctuations, whereas small β values represent the opposite situation (short-term variations).

In Fig. 1 we compare the standard and the general approach. Even though the computing cost of the general formulation is higher than that of the standard approach, this formulation manifests several advantages. We can deal with irregular sampling in time of noise correlations; therefore, this technique is more efficient when the dataset is complex. Also, long-term or short-term trends are obtained directly from the inversion process rather than fitting the velocity change time series with polynomial functions, as in the standard approach (Brenguier et al. 2008b).

In this work we consider station pairs independently to obtain single time series of velocity fluctuations but we can also invert several raypaths at the same time to achieve a more homogeneous and general trend of seismic velocity variations rather than averaging over different time series from different station pairs. By concatenating doublet measurements from different station pairs for a global inversion, the robustness of retrieved velocity changes improves by minimizing the effect of missing data.

In the following, we describe synthetic tests to explicit the advantages and limits of that novel approach.

3 SYNTHETIC TESTS

In this section we analyze how the stability of noise-correlations influences the reconstruction of velocity change time series for different cases. Specifically, the causes that we want to study are:

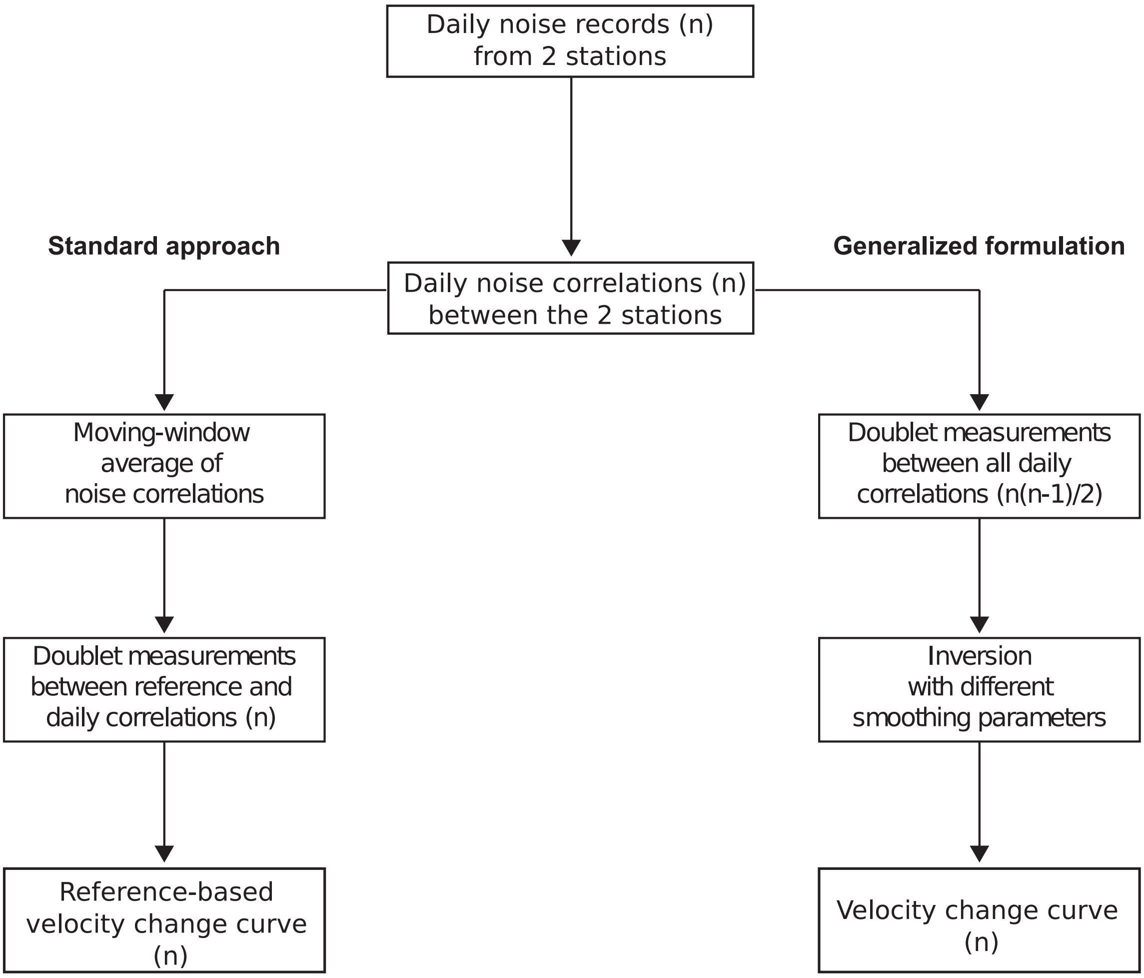

Figure 1. Workflow diagram showing the main steps of the standard approach and the general one. n is the number of days.

- Seasonal-type trends which produce long-term periodic-type velocity changes, i. e., long-term variations.
- Rapid transient changes similar to those produced as a result of an earthquake or a volcanic eruption. The effect of those changes in the noise correlations is the retrieval of a sudden velocity drop (short-term variations), corresponding to a permanent or almost permanent velocity change.
- Transient strong perturbations of the noise correlations due to a local source emission, such as the perturbation induced by episodic volcanic tremor (Droznin et al. 2015). The consequence is a sudden velocity drop and a sudden recovery, producing short and medium-term velocity fluctuations.

We use a synthetic test approach by artificially stretching noise cross-correlations in order to simulate synthetic velocity changes. We further degrade the quality of the dataset of noise cross-correlations by adding different levels of random noise in order to simulate unstable to stable noise cross-correlations. We then apply our novel method for reconstructing velocity changes and finally compare the 'expected' and the 'reconstructed' time series of velocity changes. We also study the improvement of averaging the inverted times series of velocity changes for different station pairs.

The Pearson correlation coefficient (coherence) between two synthetic noise cross-correlations is used as a proxy for the quality of the associated doublet measurement and used to built the $\mathbf{C_d}$ matrix of data weighting. The average of all Pearson correlation coefficients between all pairs of noise cross-correlations (CCFs) is referred as the coherence level. This value describes the level of added random noise by varying from 0 (totally incoherent noise CCFs) to 1 (no random noise added).

3.1 Long-term periodic-type fluctuation test

In this section we refer to velocity change measurements at a crustal scale using micro-seismic noise correlations in the frequency range from 0.1 to 1 Hz. However, this approach can be extended to other frequency domains and sources of seismic noise.

By stretching a single arbitrary CCF with different daily velocity changes (referred as expected velocity changes henceforth), we simulate daily synthetic CCFs. Fig. 2, right panel shows the expected velocity changes that we apply and that simulate long-term periodic-type velocity changes. The other panels of Fig. 2 show examples of synthetic CCFs with different levels of noise. The different panels of synthetic CCFs are associated with a coherence level (referred as *coh* in the figures), that is a measure of the level of added random noise. By adding random noise we are 'hiding' the original time series of velocity changes that we want to reconstruct after inversion, i. e., the 'expected' velocity changes.

We obtain the data vector of velocity changes, **d**, by applying a MWCS analysis between all possible pairs of CCFs. For *n* daily cross-correlation functions, we estimate $\frac{n(n-1)}{2}$ doublet measurements. We measure doublets in windows of 10 s centered between the direct surface-wave arrival time and a lapse time of 70 s in the coda. Moving windows are overlapped by 80 %. We finally perform the inversion for retrieving daily velocity changes (vector **m**). As we are studying long-term variations, we use a large β values to retrieve $d\nu/\nu$ series, $\beta = 1000$, while α decreases with the coherence level, from $\alpha = 5000$ to $\alpha = 100$.

In Fig. 3 we compare the reconstructed time series of velocity changes obtained from the synthetic CCFs of Fig. 2 with the expected one. The more noise we add, the less coherence level we have and the more the reconstructed time series of velocity changes differ from the expected velocity changes.

We test three different levels of expected velocity changes (Fig. 4a) to achieve the final time series of velocity changes. The peak amplitude of the expected velocity change curve 1 is 0.001 %, while expected velocity change curves 2 and 3 present peak amplitudes of 0.005 % and 0.01 %, respectively. For Figs. 2 and 3 we use the expected velocity curve 3.

Fig. 4b shows the correlation coefficients between the reconstructed and the expected time series as a function of the coherence levels, for the three different expected velocity changes. By considering greater velocity change amplitudes (expected velocity change curve 3), we achieve higher similarity between the reconstructed time series of velocity changes and the expected ones, for the same level of noise.

To simulate the averaging of inverted time series of velocity changes over different station pairs, we build different station pairs with synthetic stretched cross-correlation data. We apply the same velocity change stretching procedure but with different random noise to simulate different synthetic station pairs. We use the expected velocity change curve 3 and a fixed high level of noise ($coh = 0.06$) to simulate up to 50 different synthetic station pairs. After obtaining the 50 reconstructed velocity change curves, we average them to study the improvement. N_{sta} is the number of averaged curves of reconstructed velocity changes.

Fig. 5a shows higher correlation between time series (Fig. 5b) with higher number of averaged curves, N_{sta}. With this low coherence level we can retrieve a correlation coefficient between the inverted and expected velocity change curves of more than 0.9 for $N_{sta} = 50$ and for $N_{sta} = 20$ we already reach a correlation coefficient of 0.7. Fig. 5b shows the averaged curve for $N_{sta} = 50$ and the expected velocity change curve 3. In general, it is thus recommended to average seismic velocity changes over at least 20 station pairs when the noise cross-correlations are so unstable. Although Fig. 5a shows a correlation coefficient of 0.22 for $N_{sta} = 1$, in Fig. 3 we show a greater correlation coefficient, 0.41, for the same coherence level, $coh = 0.06$, because we picked one of the best examples to show.

With this test we have studied how our method resolves the effects of a seasonal-type trend. To recover long-term periodic-type fluctuations, we choose a high β value, $\beta = 1000$, while depending on the coh of the CCFs, we use different values for α, choosing lower values for lower coh, to fit better the expected velocity change curve. With the use of three different expected velocity change curves, we also have seen that the reconstructed time series of velocity changes is closer to the expected one when the velocity change amplitudes to retrieve are greater. On the other hand, it is also important to note that, although there is a great improvement when averaging over different station pairs (Fig. 5a, from a correlation of 0.22 for $N_{sta} = 1$ to 0.87 for $N_{sta} = 50$, increasing then the correlation by a factor of 3.9), the reconstructed velocity changes will remain underestimated (there is no convergence to 1, Fig. 5a, and the amplitude of the reconstructed time series of velocity changes for $N_{sta} = 50$ is one magnitude order smaller than the expected velocity changes, Fig. 5b), probably due to an edge effect of the time series. In case of CCFs with low coh, it is recommended to average seismic velocity changes over several station pairs, at least over 20 in case of very unstable CCFs.

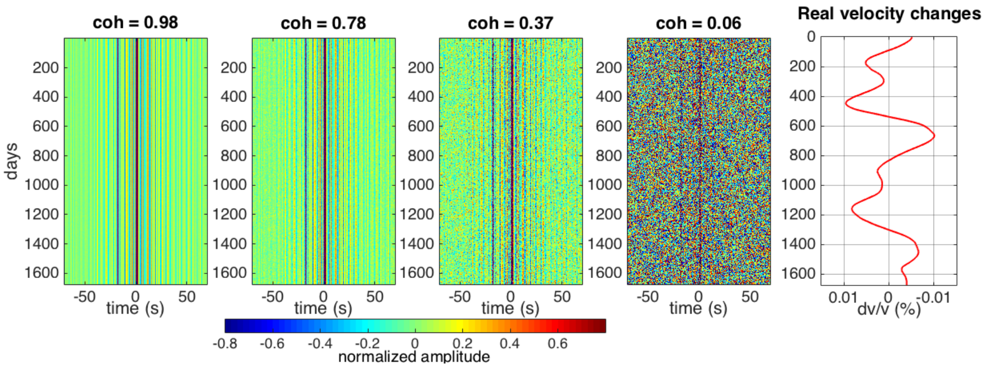

Figure 2. Examples of synthetic stretched CCFs with different levels of random noise. The coherence level (coh) is on top of each figure. On the right, expected velocity changes applied to stretch the CCFs (red curve).

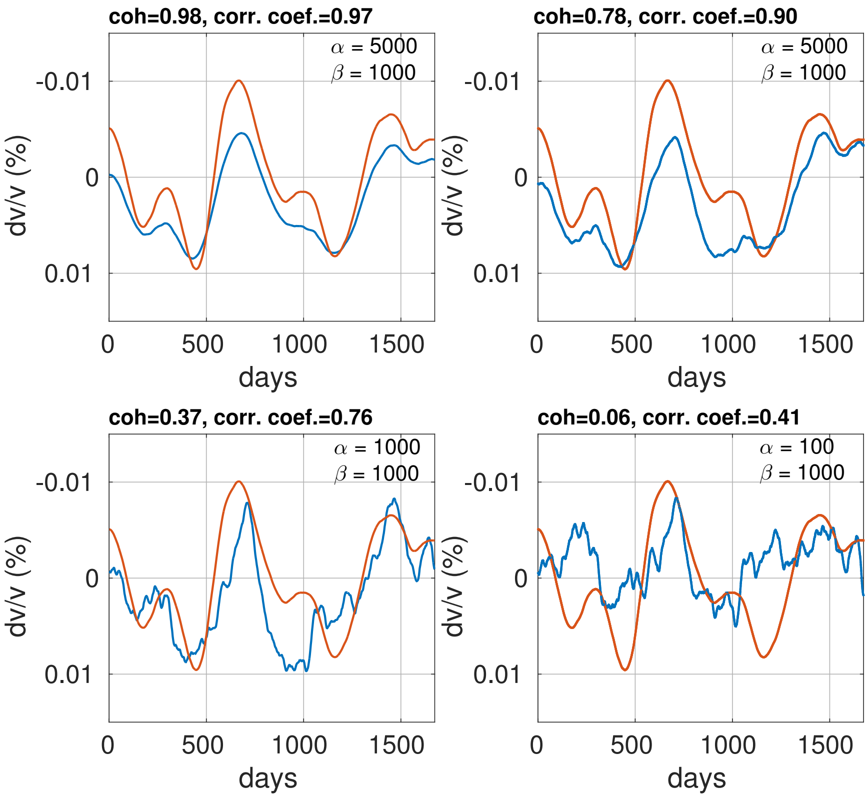

Figure 3. Reconstructed velocity change time series (blue curves) vs. the expected velocity changes (red curve) for different coherence levels. Correlation coefficients between both curves on top of each figure.

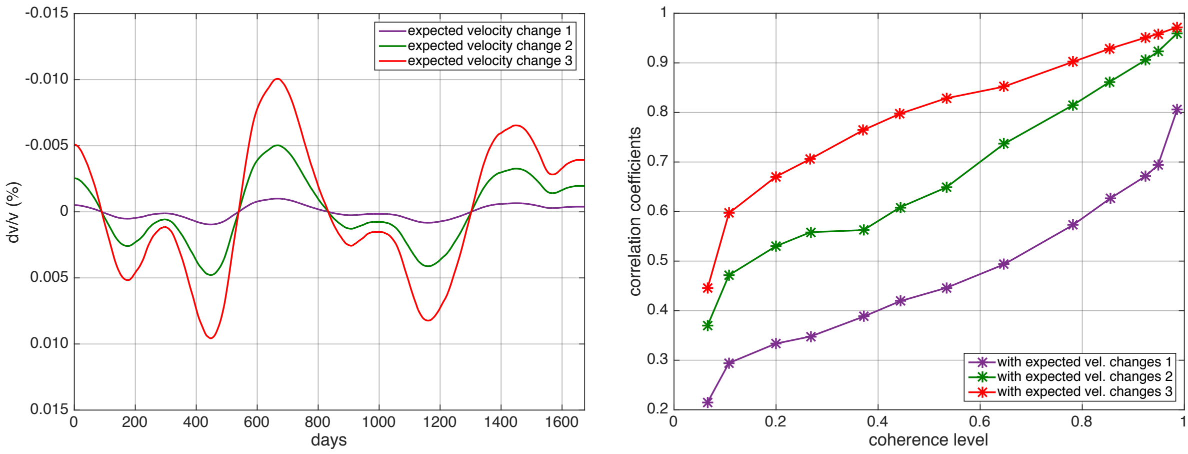

(a)

(b)

Figure 4. (a) Expected velocity change curves used in the long-term periodic-type fulctuation test. (b) Convergence curves of the coherence levels and the correlation coefficients between the reconstructed velocity change time series and the different expected velocity changes.

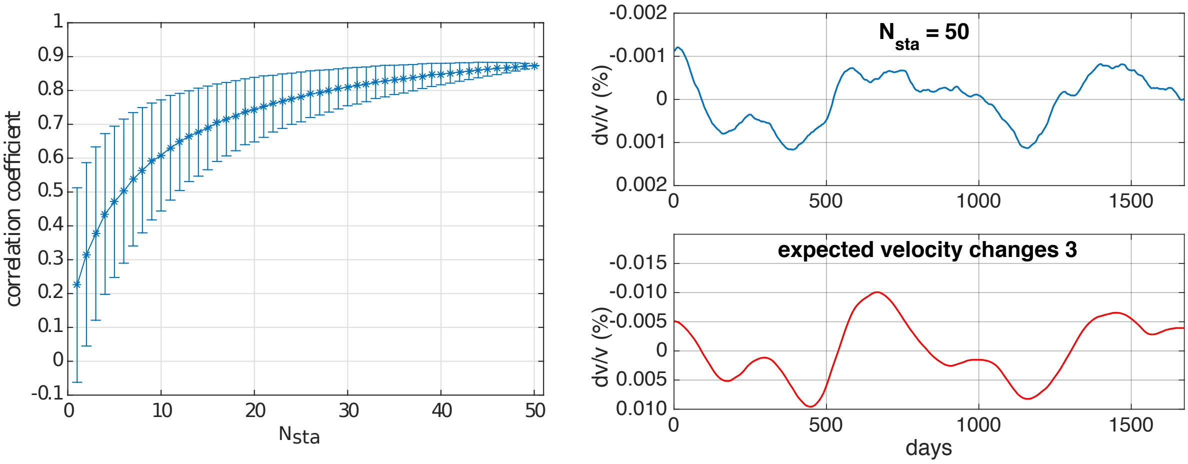

(a)

(b)

Figure 5. For a coherence level = 0.06 and the expected velocity change curve 3: (a) Correlation coefficients between the reconstructed velocity change time series and the expected velocity changes 3 as a function of the number of averaged curves of reconstructed velocity changes, N_{sta}. Associated standard deviations in blue bars. (b) Reconstructed velocity change time series for $N_{sta} = 50$ (blue) and the expected velocity change curve 3 (red).

3.2 Velocity drop test

To test the reconstruction of an abrupt, rapid change of velocity, similar to the effect of an earthquake (e.g., Brenguier et al. 2008a), we add a Heaviside step function with a velocity change of 0.05 %, to the previous expected velocity change curve 3 (Fig. 6, red curve), referred as the drop curve in this section

As we are interested in recovering the drop, we use another coefficient to study the similarity between the reconstructed time series and the drop curve instead of using the Pearson correlation coefficient. To estimate the quality of the reconstructed drop, we measure the difference between the mean velocity changes after and before the drop:

$$diff = \overline{\left(\frac{\mathrm{d}\nu}{\nu}\right)}_{after\ drop} - \overline{\left(\frac{\mathrm{d}\nu}{\nu}\right)}_{before\ drop} \tag{8}$$

We compute $diff$ for both the reconstructed velocity change curve and the expected drop curve. We then estimate the quality of the reconstructed drop by the ratio:

$$Q_{drop} = \left|\frac{diff_{reconstructed\ velocity\ change\ curve}}{diff_{drop\ curve}}\right| \tag{9}$$

Q_{drop} is 1 when perfectly reconstructed, and < 1 otherwise. In this test, we invert for time series of velocity changes by using a small β to obtain short-term variations, $\beta = 5$ and we avoid a smoothing factor ($\alpha \approx 0$).

Fig. 6 shows the retrieved drops for several examples of different coherence levels. As the level of noise increases (*coh* decreases), the drop in the reconstructed time series of velocity changes becomes smaller until it almost disappears (when the coherence level is nearly zero).

Fig. 7 shows the convergence of Q_{drop} for different coherence values of the synthetic cross-correlations.

We also study the improvement of averaging the reconstructed velocity change curves over different station pairs. For a fixed coherence level of 0.37, we study the convergence of the retrieved drop by increasing N_{sta} (Fig. 8a). Interestingly, by averaging more reconstructed velocity changes, we smooth the sharp short-term fluctuations while the recovered drop remains the same. We also estimate the increasing Signal to Noise Ratio (SNR) associated with the increasing number of averaged synthetic functions, N_{sta}, as:

$$\mathrm{SNR} = \frac{level\ of\ recovered\ drop}{\mathrm{rms}(averaged\ \frac{\mathrm{d}\nu}{\nu}\ curve)} \tag{10}$$

with rms($averaged\ \frac{\mathrm{d}\nu}{\nu}\ curve$) being the root mean square of velocity change mean curve for each N_{sta} (Fig. 8a).

A way to increase the coherence between CCFs and, therefore, to improve the temporal resolution of the velocity change measurements, is the use of denoising methods such as Curvelet filtering (Stehly et al. 2015) or Wiener filtering. We applied a FIR Wiener filter to our CCFs without obtaining a great improvement in the reconstructed velocity changes, probably because this technique affect only to the amplitude of the frequency spectrum whereas the method presented in this article only uses the phase of the signal.

For a coherence level of 0.37 and $N_{sta} = 50$, we get a Q_{drop} of 0.6 and a SNR of 38 (Figs 8a and 8b). Again, it is interesting to note that, for highly unstable correlations (e.g., coh=0.37), averaging over different station pairs will not improve the value of the level of the velocity drop that will remain underestimated. Averaging over different receiver pairs will however improve the SNR of the recovered velocity changes and thus allow a better estimate of the timing of the velocity drop.

To summarize, the reason for this test was to check the effect of a sudden change in the structure, similar to the effect of a volcanic eruption or an earthquake. Simulating a transient change, we can infer short-term velocity fluctuations. We used $\beta = 5$, avoiding the smoothing ($\alpha \approx 0$), in order to study just the effect of the velocity drop with our method. The lower the coh of the CCFs considered, the smaller the velocity drop in the reconstructed time series of velocity changes. We have seen that this velocity drop remains underestimated, even averaging over several station pairs, although the improvement associated to the SNR of the reconstructed velocity changes allows us to set better when the velocity drop happens.

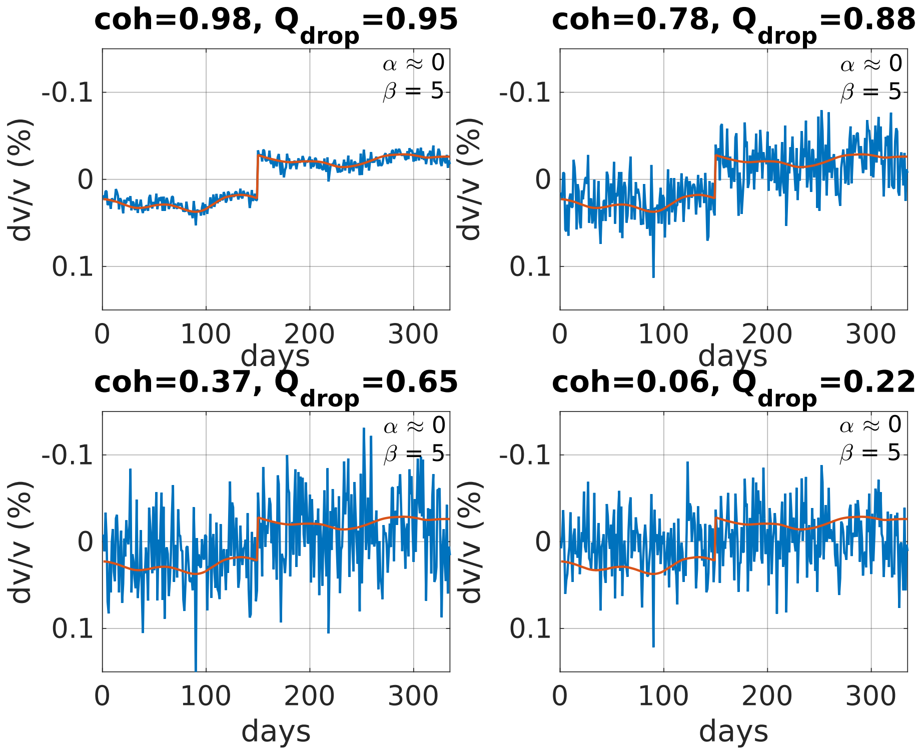

Figure 6. Reconstructed velocity change time series (blue curves) vs. the drop curve (red curve) for different coherence levels. Q_{drop} on top of each figure.

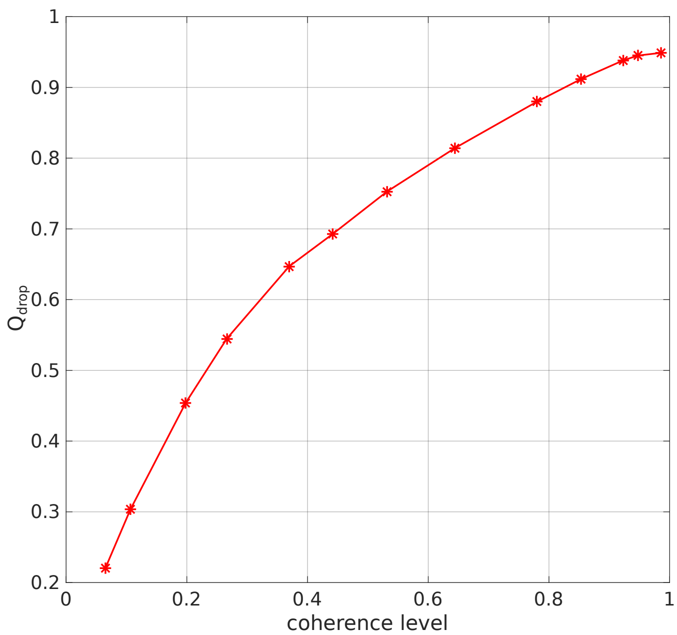

Figure 7. Convergence curve between the coherence levels and the percentage of the recovered drop.

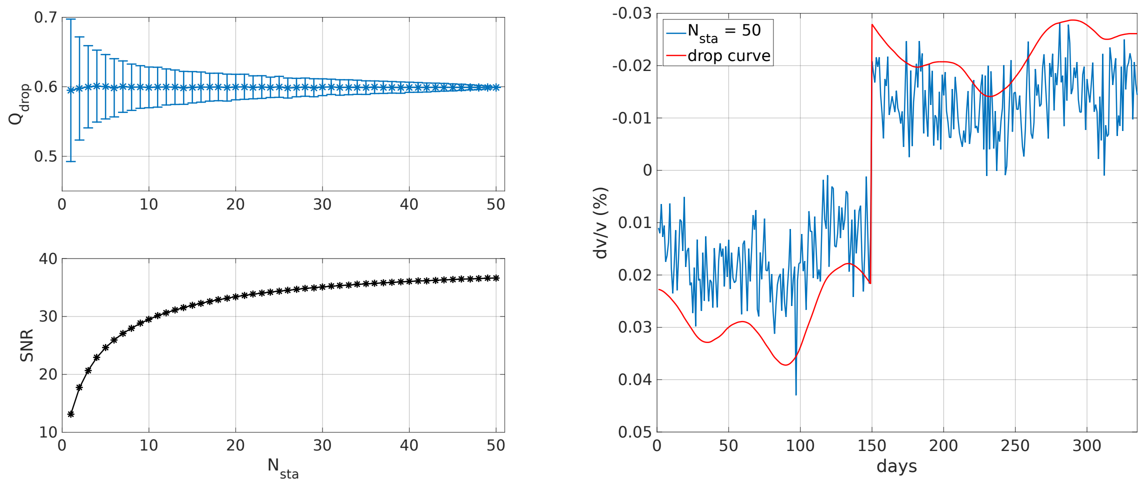

(a) (b)

Figure 8. For a coherence level = 0.37: (a) Percentage of recovered drop (associated standard deviations in blue bars) and signal-to-noise ratio (SNR) (black curve) as a function of the number of synthetic averaged functions (N_{sta}). (b) Reconstructed velocity change time series for $N_{sta} = 50$ and drop curve.

3.3 Transient noise perturbation test

In this test we study the effect of an episodic strong change in the noise-correlation shape induced by a strong noise source change, e.g., a passing storm or a episodic volcanic tremor. This last situation has been described by Ballmer et al. (2013) and Droznin et al. (2015) in case of noise-correlations affected by the occurrence of low-frequency volcanic tremor. We herewith test the ability of our method to recover robust velocity changes in this situation.

To compute the synthetic stretched CCFs, we consider two real normalized CCFs, one during a non-tremor period (C_1) and the other during a tremor period (C_2). Basically we consider C_1 as the true GF and C_2 as a pure tremor-related bias. With both, we make two new averaged correlations: $C_3 = 0.8 \times C_1 + 0.2 \times C_2$ and $C_4 = 0.8 \times C_2 + 0.2 \times C_1$, corresponding to a calm period (C_3) and to a tremor period (C_4), respectively. We concatenate N_1 correlations C_3, N_2 correlations C_4 and again N_1 correlations C_3, N_1 and N_2 being random numbers of daily CCFs. Then, we stretch the CCFs and add different levels of random noise to these correlations in the same way than in previous tests.

Fig. 9a is an example of synthetic stretched CCFs with a certain level of random noise ($coh = 0.54$). We see clearly the differences in the shape of CCFs corresponding to a calm period, C_3 (from $n = 1$ to $n = 30$ and from $n = 90$ to $n = 120$ in Fig. 9a), and to a tremor period, C_4 (from $n = 30$ to $n = 90$ in Fig. 9a). Fig. 9b is the associated correlation coefficient matrix of Fig. 9a which represents all Pearson correlation coefficients between all pairs CCFs. We observe the lower correlation between CCFs of the tremor period comparing with the calm periods.

Fig. 10 shows some examples of the resulting reconstructed time series of velocity changes for the maximum coherence level of 0.85 and for some lower ones, where the coherence level decreases due to the increased level of random noise in the synthetic CCFs. We also plot the expected velocity curve for comparison. In the cases of a high coherence level, we observe a double velocity drop in the recovered synthetic velocity change curves (between days 30 and 90) due to the three different parts of the synthetic functions, i.e., the first N_1 days (calm period), the next N_2 days (tremor period) and the last N_1 days (calm period again) (Fig. 9). We explain this double velocity drop by looking at the correlation coefficient matrix (Fig. 9b). Since the correlation coefficients of the noise CCFs between the calm and the tremor period are very low (Fig. 9b), our method treats these data segments separately and thus generates this baseline difference between the two periods. Therefore, these artificial velocity drops are artefacts from our method. The double velocity drop observed in the reconstructed time series is hidden when the level of noise increases.

Even more interesting, when we increase the number of inverted synthetic time series of velocity changes for a low coherence value to study the improvement associated with averaging over different station pairs (Fig. 11a), we see clearly the improvement in the similarity between the inverted curves and the expected one (Fig. 11b). This is because only C_1, the medium, is coherent and the noise source perturbation is not seen the same way by all receiver pairs. This means that for some station pairs, the double velocity drop induced by the tremor has, sometime, opposite sign which, simply, cancels out while summing over different receiver pairs.

We have tested in this subsection the effect of a transient and sudden local source emission, producing short to medium-term fluctuations. Since we are interested on evaluating the sudden velocity drop and sudden recovery in the reconstructed time series of velocity variations, we consider $\beta = 5$ and $\alpha \approx 0$, as in the previous test. We have observed artificial velocity drops produced by our method, visible only when the coh of the CCFs is high and hidden with low coh.

In conclusion, there are two approaches in the situation of strong noise perturbations. In case the coherence level between the noise CCFs is high, it might worth correcting for the artificial baseline difference after the inversion to retrieve proper velocity changes. When the coherence is low, the only way to retrieve a proper velocity change curve is to average over sufficient station pairs (50 in that example).

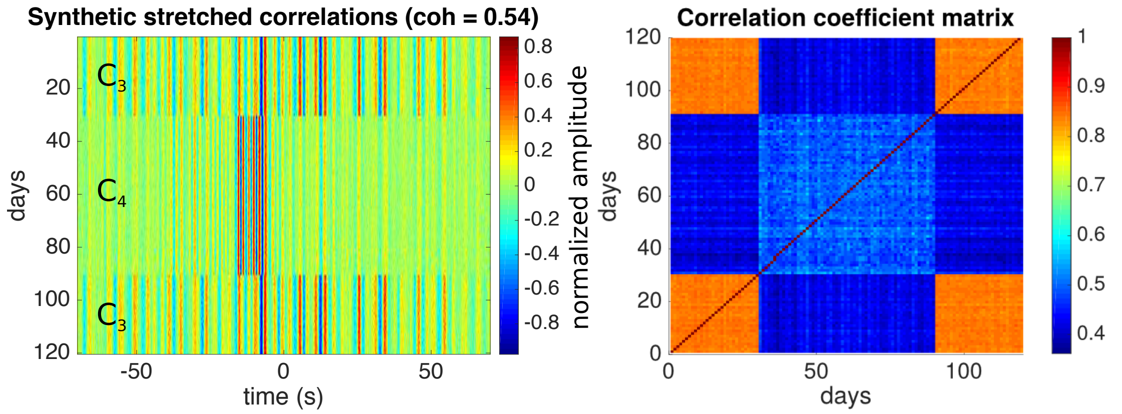

(a) (b)

Figure 9. (a) Example of a normalized synthetic stretched CCFs of the tremor test with a random level of noise (shown for a coherence level between CCFs of 0.54). (b) Correlation coefficient matrix associated to the doublets.

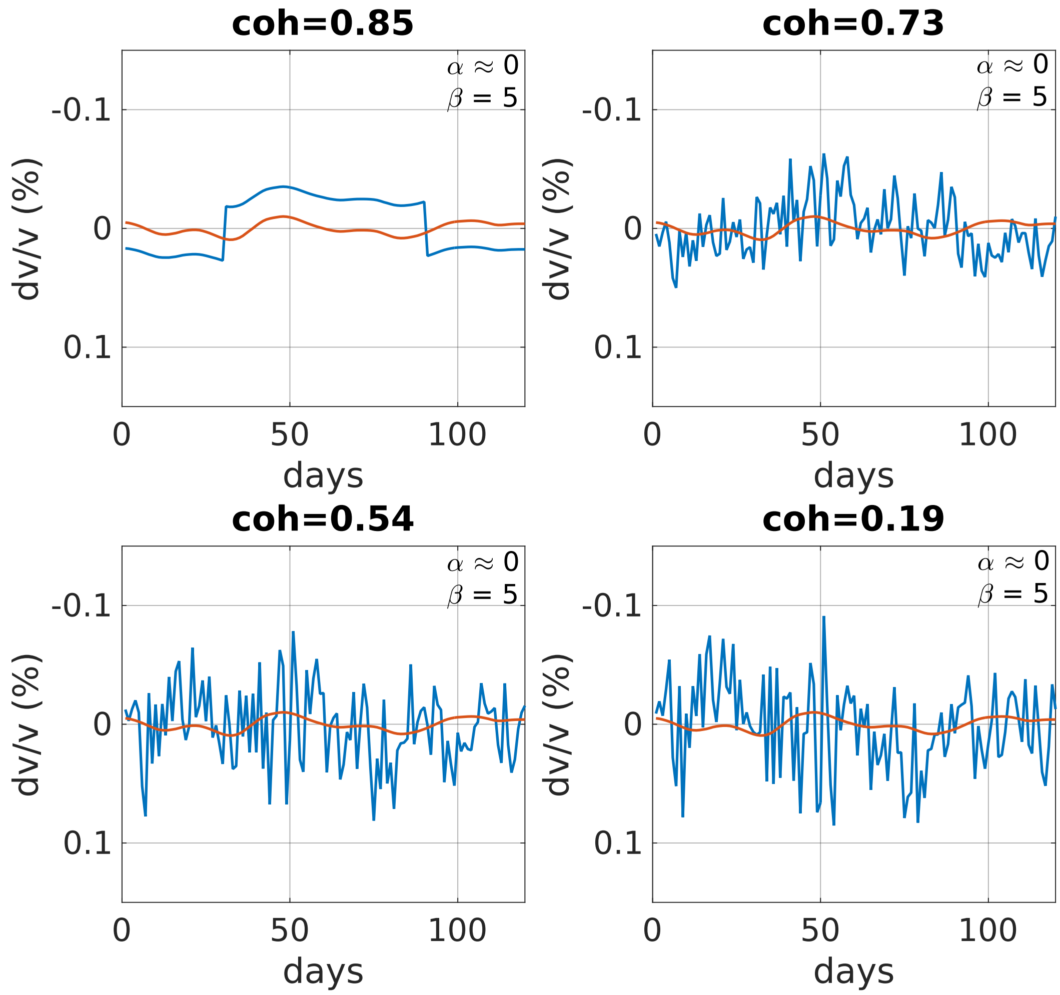

Figure 10. Synthetic velocity change time series (blue curves) vs. the expected velocity changes (red curve) for different coherence levels.

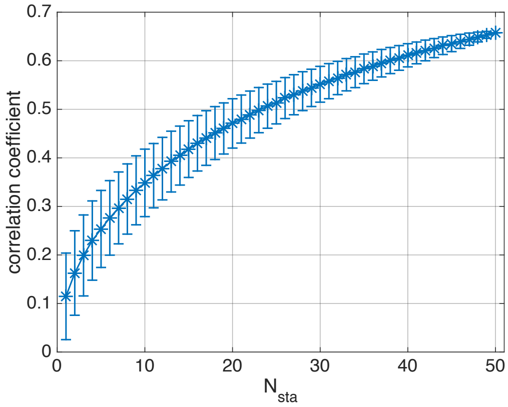

(a)

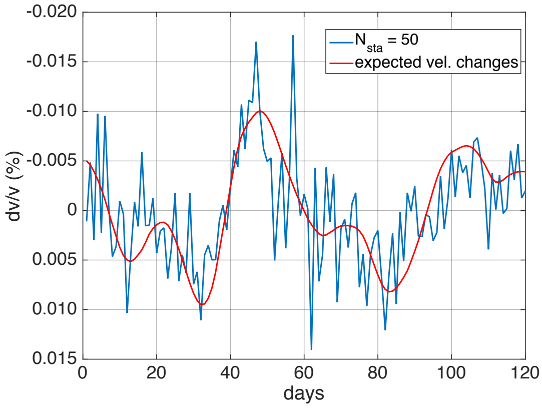

(b)

Figure 11. For a coherence level = 0.54: (a) Correlation coefficients between synthetic velocity change curves and the stretching curve as a function of the number of synthetic averaged functions (N_{sta}). (b) Reconstructed velocity change time series for $N_{sta} = 50$ compared to the expected velocity changes (red curve).

4 APPLICATION TO REAL DATA

With synthetic tests, we have established a general framework to identify and interpret long-term periodic-type velocity changes from seasonal-type trends, rapid velocity drops, due to transient changes, and sudden velocity drop and recovery as an effect of transient and sudden local source emissions. We have analyzed the effect of the regularization parameters and the averaging over station pairs for the three different cases. Now, we apply the method to a complex dataset of noise cross-correlations at Klyuchevskoy volcanic group (Kamchatka), hampered by lose of data and the presence of highly non-stationary seismic tremor.

4.1 Klyuchevskoy volcanic group

The Klyuchevskoy volcanic group (KVG), located in Kamchatka, is one of the most active clusters of subduction-zone volcanoes in the world, where the annual rate of explosive eruptions is three to five (Schneider et al. 2000). The KVG has an averaged extension of 70 km and 13 stratovolcanoes. It includes active volcanoes such as Klyuchevskoy, Krestovsky, Ushkovsky, Bezymianny and Tolbachik. The Klyuchevskoy Volcano, the most outstanding volcano with 4750 m high, is associated with the emission of basaltic and basaltic-andesitic lavas and it has a mean eruptive rate of 1 m^3 s^{-1} over the last 10 kyr (Fedotov et al. 1987). Two other active volcanoes, Shiveluch and Kizimen, are located only 60 kilometers north and south, respectively, of KVG.This cluster of volcanoes is located off the edge of a tectonic junction: the Pacific Plate is subducting down the Aleutian Trench and also moving under the Okhotsk Plate. The high volcanic activity is also a consequence of the Hawaii–Emperor Seamount chain that terminates in the Kuril-Kamchatka Trench. Geodynamic models that have been proposed to explain the exceptional activity of the KVG include fluid being released from the thick, highly hydrated Hawaii–Emperor Seamount crust (Dorendorf et al. 2000), mantle flow around the corner of the Pacific plate (Yogodzinski et al. 2001), and recent detachment of a portion of the subducting slab (Levin et al. 2002; Levin et al. 2005).

The volcanic activity of the KVG leads to the generation of strong volcanic tremors (Gordeev et al. 1990) with sources located very close to the surface and at depth near the crust mantle boundary (Shapiro et al. 2017a) which spoil the ambient noise cross-correlations. We use the information of Droznin et al. (2015) and Soubestre et al. (2017) about detection of these signals and about location of their sources in Klyuchevskoy volcanic group to recover seismic velocity fluctuations in this region, since we use the same dataset of noise cross-correlations as well.

The particular tectonic settings surrounding KVG and its strong eruptions with high seismic activity (e.g. Senyukov et al. 2009; Zharinov & Demyanchuk 2009; Ozerov et al. 2013) enable many seismic tomographic surveys (e.g. Slavina et al. 2012; Koulakov et al. 2013; Lees et al. 2013) and receiver function analysis to study the internal structure of the KVG (Nikulin et al. 2010).

Tomographic studies on the KVG reveal a extremely high Vp/Vs ratio (up to 2.2), below 25 km deep. This feature can acts as a channel which brings deep mantle materials from the mantle to the bottom of the crust and is responsible for all volcanic activity in the KVG (Koulakov et al. 2013).

Our study period goes from January 2009 to July 2013 in which both the Klyuchevskoy and the Tolbachik volcanoes erupted. From the Klyuchevskoy volcano, two eruptions took place. The first one started in June 2008 and the volcanic activity ceased at the end of January 2009. The second Klyuchevskoy eruption goes from July 2009 to December 7, 2010. Spatterings of hot magma started on August 2, 2009. The summit eruption activity were characterized by weak ash emissions (less than 300 m of height) although in 2010 the ash emissions were stronger (9 km of height). The eruption decreased at the end of 2010. All the recorded Klyochevskoy summit eruptions are characterized by a gradual growth of activity (Senyukov 2013). A detailed analysis of records of volcanic tremors has been used by Soubestre et al. (2017) to identify two different stages of the 2009-2010 Klyuchevskoy eruption with the stronger second stage starting approximately in June 2010.

The last eruption is the fissure eruption of the Tolbachik volcano (2012-2013). The 2012-13 Tolbachik eruption starts on November 27, 2012 corresponding to an eruptive tremor (Fig. 16) due to a first magma migration (Caudron et al. 2015). The Tolbachik regional zone of cinder cones is 900 km^2 in size and 70 km long. Before last eruption (2012-2013), historical eruptions in Tolbachik zone occurred in 1740, 1941 and 1975-1976 (Gordeev et al. 2013).

The three eruptions are characterized by emissions of seismic tremors (Gordeev et al. 1990; Droznin et al. 2015; Shapiro et al. 2017a).

4.2 Data

We use continuous records from a total of 18 three-component seismic stations (Fig. 12) of the seismic network deployed by the Kamchatka Branch of the Geophysical Service (KBGS) of the Russian Academy of Sciences (Chebrov et al. 2013). Every component of the stations presents a CM-3 short period sensor. We analyze data recorded continuously between 1 January 2009 and 7 July 2013.

Records are digitalized at 128 samples per seconds and downsampled to 8 samples per second. Cross-correlations are calculated in 24-h long segments. We pre-process the continuous records following the method described by Bensen et al. (2007). We choose a spectral band between 0.08 – 0.7 Hz because, after 0.7 Hz, the correlations are too much affected by volcanic tremor correlation signals. After whitening, 1-bit normalization suppresses high-amplitude data, such as earthquake signals, and emphasizes low-amplitude data, such as ambient seismic vibrations. Volcanic tremors still act as potential biasing signals perturbing the reconstructed GF, after reducing persistent signals from localized sources with pre-processing. Then, we compute daily cross-correlation functions for all possible station pairs. We work with coda waves of daily CCFs between the vertical-component records of the station pairs (Rivet et al. 2014).

For passive monitoring techniques, both the continuity of the records and the good quality of data are important. For this reason, we do first a quality check of the daily cross-correlation functions for each possible seismic station pair, 209 pairs in total. We visually inspect all CCFs of each station pair to rank them in different groups according to the quality of the recordings. Taking into account the continuity and regularity over time of the CCFs where coda waves are clearly distinguished, we consider three quality groups, from best to worst: A, B and C. We can apply our method to the CCFs of the station pairs ranked in groups A and B but not to those of group C.

We work with station pairs ranked in group A, there are 23 in total. Fig. 13 shows an example of daily CCFs computed for a station pair ranked in group A with its associated correlation coefficient matrix. The periods with highest correlation coefficients correspond to the first two-thirds of 2010 and to 2013. While most of the station pairs of the group A are in the vicinity of Klyuchevskoy and Tolbachik volcanoes, three station pairs (from stations BDR, SMK and SRK) are farther away from the rest, in the vicinity of the Shiveluch volcano (Fig. 12). Because of this, in our study we separate these three stations near Shiveluch from the others. By the MWCS analysis, we compute all the doublets for the 23 station pairs.

Figs 14 and 15 show correlation coefficient matrices for each station pair ranked with A. We can see different patterns in correlation coefficients if we compare the main group of station pairs (Fig. 14) with the northern group (Fig. 15). All pairs show a strong correlation in the second half of 2010 and in 2013, matching with the ongoing Klychevskoy and Tolbachik eruptions (Droznin et al. (2015), fig. 5), respectively. Highest correlation values are observed between the stations of the main group (Fig. 14).

Daily averaged levels of tremors are shown in Fig. 16, determined by the KBGS operators. The strongest tremor activities of both volcanoes also match with the highest correlation coefficients between CCF (Fig. 14).

Before the inversion, we reject the doublets where the associated correlation coefficients (Figs 14 and 15) are smaller than 0.3. Thereby, we ensure the recovered temporal velocity variation curves tend towards zero for days with bad quality recordings.

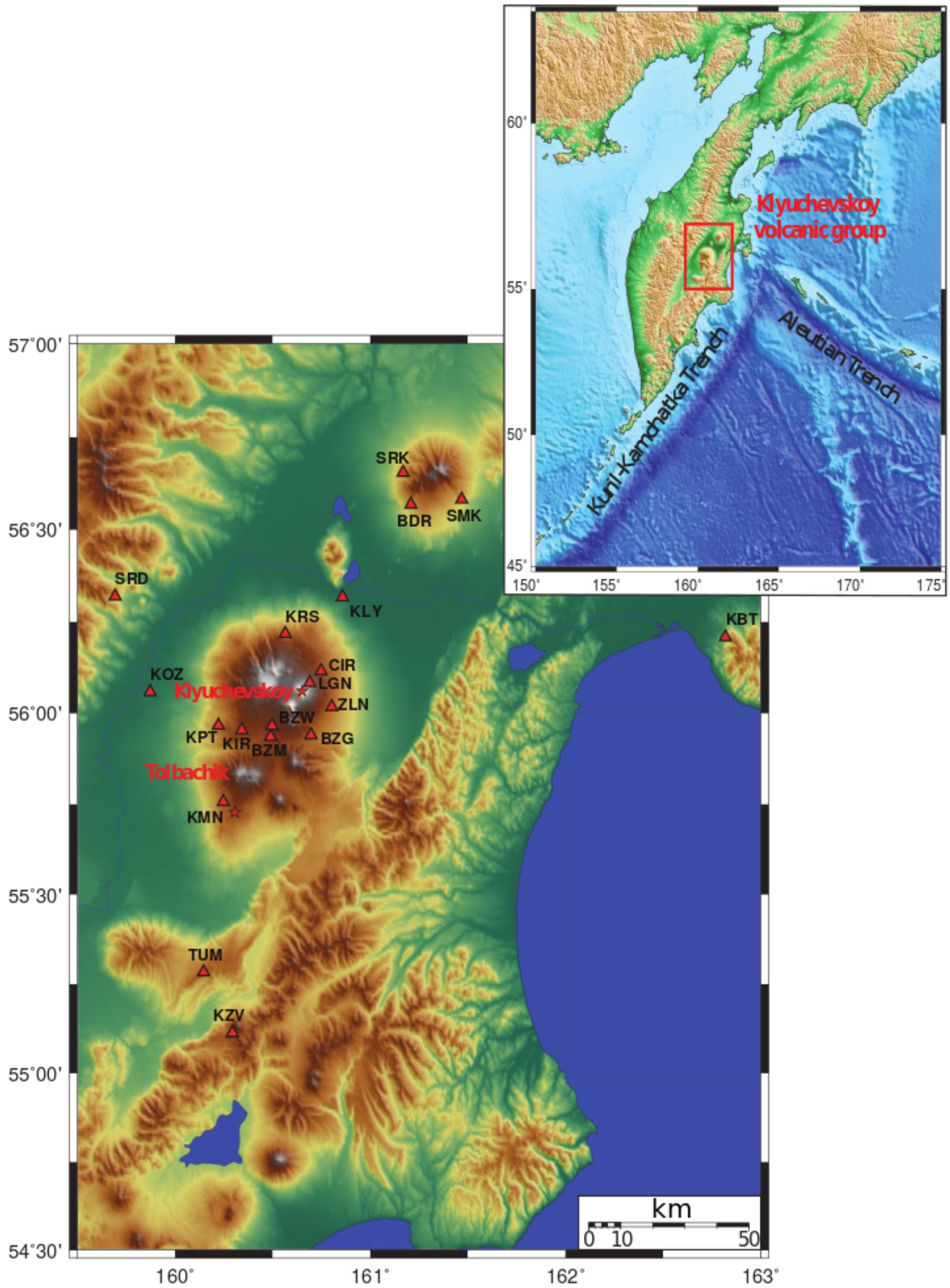

Figure 12. Topographic map of the Klyuchevskoy group of volcanoes in Kamchatka peninsula with positions of seismic stations. Red starts are the eruptive centres of the 2009-2010 Klyuchevskoy and of the 2012-2013 Tolbachik volcanoes.

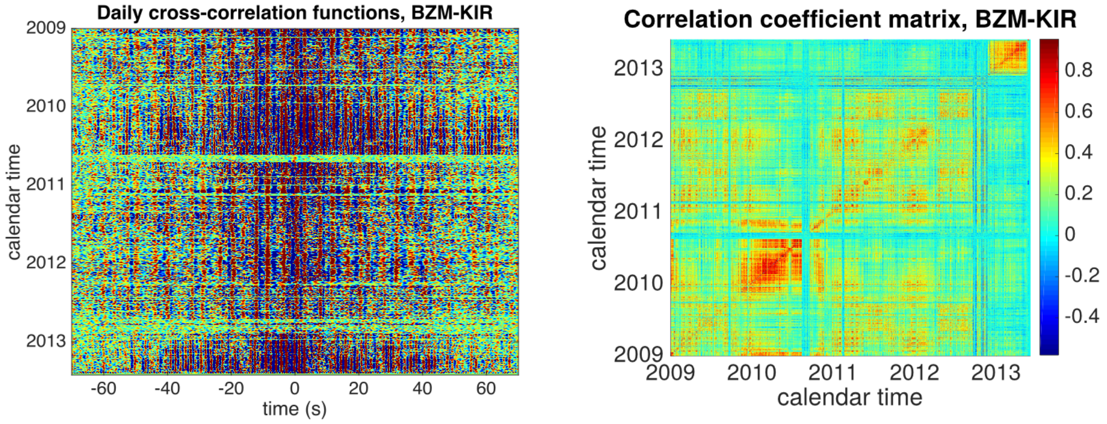

(a) (b)

Figure 13. (a) Daily CCF computed from station pair BZM-KIR. (b) Correlation coeffient matrix associated to the doublets of the station pair BZM-KIR.

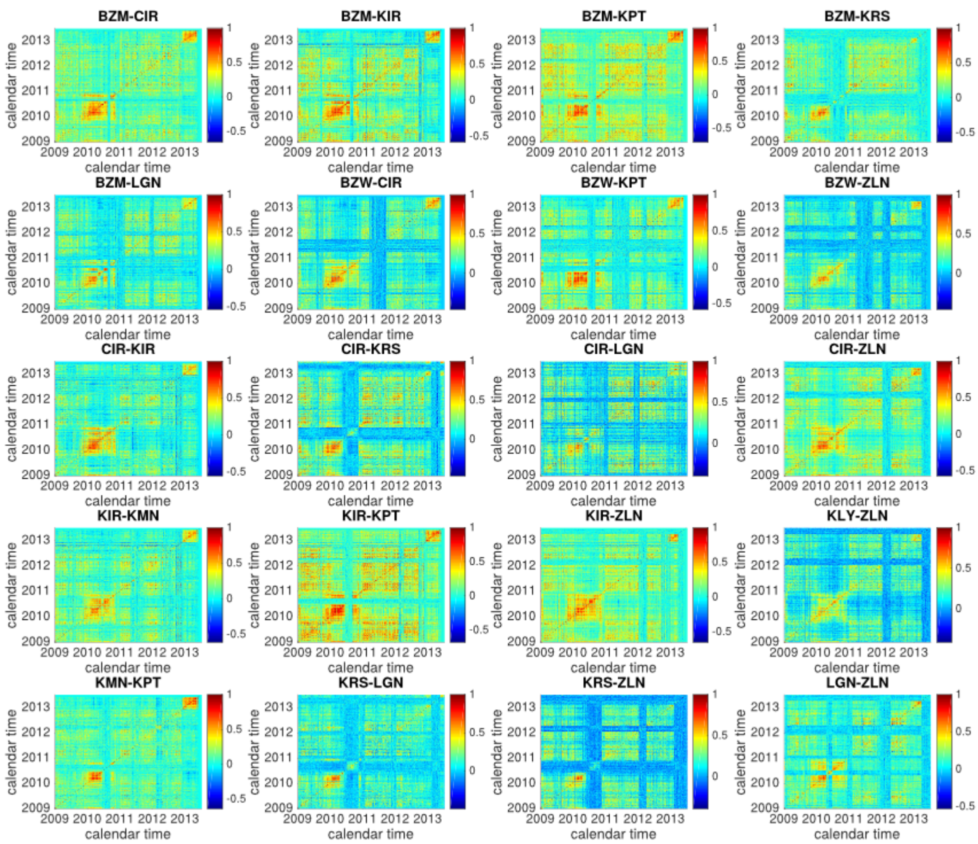

Figure 14. Correlation coefficient matrices between all daily CCF from January 2009 to August 2013 associated to 20 station pairs of group A located in the vicinity of Klyuchevskoy and Tolbachik vocanoes.

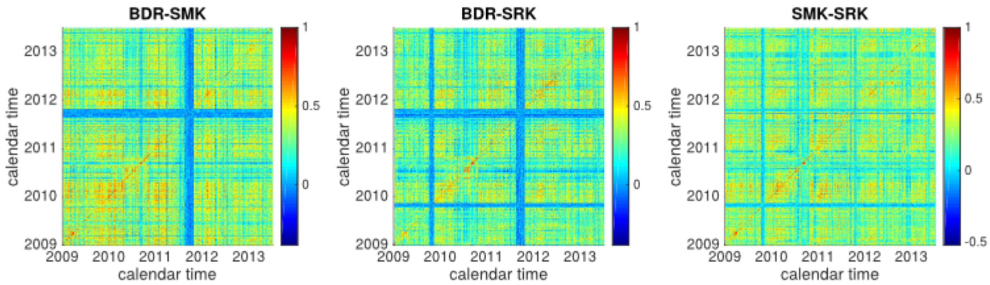

Figure 15. Correlation coefficient matrices between all daily CCF from January 2009 to August 2013 associated to the station pairs of group A located in the vicinity of Shiveluch.

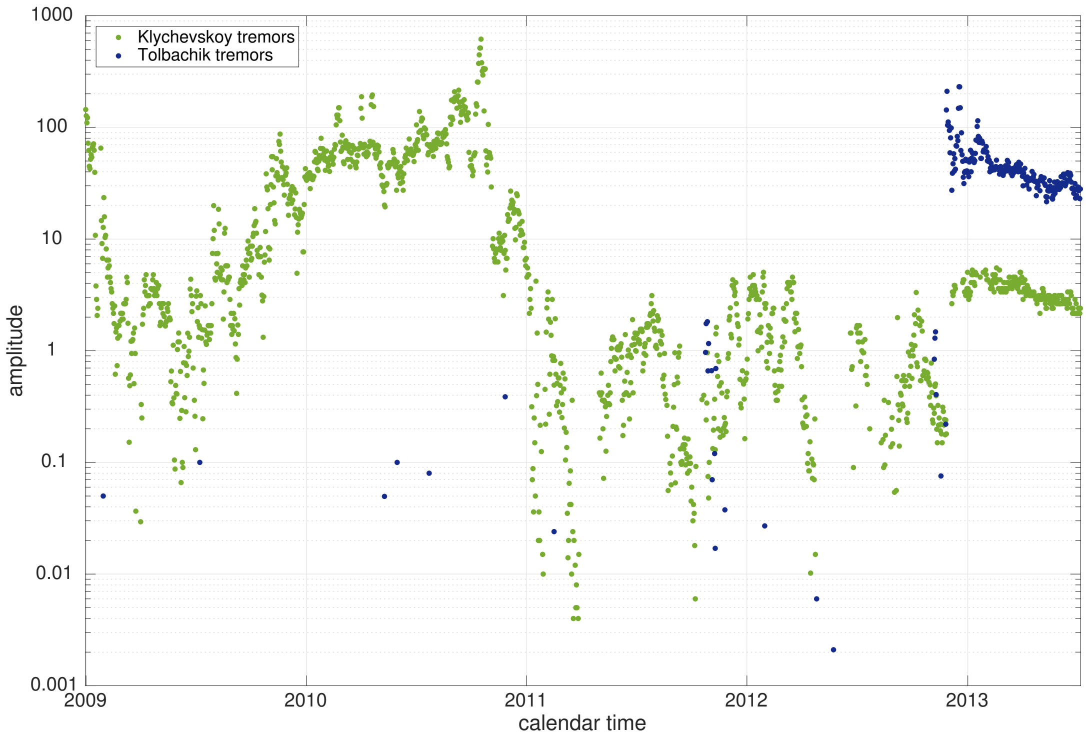

Figure 16. Normalized tremor amplitudes for Klychevskoy (green) and Tolbachik (blue) volcanoes.

4.3 Results

We show averaged velocity change time series reconstructed from CCFs of the quality group A. We average independently the stations near Shiveluch (3 station pairs) (Fig. 17) and the main group of station pairs (20 pairs in total) (Fig. 18) near Klyuchevskoy because the velocity changes associated with these two volcanoes can be very different. We compute raw relative velocity changes for all station pairs and average all curves. The parameters used for the inversion regularization are $\beta = 5$ and $\alpha = 100$. The mean coherence level of the CCFs considered in the inversion after rejecting correlation coefficients smaller than 0.3 (Figs 14 and 15), is 0.41 for both cases of averaged station pairs (3 station pairs near Shiveluch and 20 station pairs of the main group of stations).

To converge toward the actual relative velocity changes of the medium, we need to retrieve a stable trend due to long-term variations (LTV). We compute reconstructed velocity change time series from all considered station pairs with a large β value ($\beta = 1000$) to obtain precise velocity change curves that avoid short-term variations (STV). The value of the ponderation coefficient is the same than before, $\alpha = 100$. After obtaining all the individual LTV, we average them all to get the general trend.

We also plot the eruptive periods in the background of Figs 17 and 18, in green (Klyuchevskoy eruptions) and blue (Tolbachik eruption), overlaid with the reconstructed time series of velocity changes.

The maximum peak-to-peak amplitude of the retrieved LTV and the raw relative velocity changes, i.e., STV + LTV, is about 0.02 % (Fig. 18) which corresponds to the magnitude order of the amplitude of the expected velocity change curves used in sections 3.1 (Fig. 4a, expected velocity curve 3), 3.2 and 3.3. Regarding the inversion parameters, we use those tested in the synthetics: $\beta = 5$ for STV and $\beta = 1000$ for LTV. We keep the same ponderation coefficient for both cases: $\alpha = 100$. Comparing the results with the synthetics, for the mean coherence level obtained, 0.41, the correlation with the expected velocity change curve is 0.77 for long-term periodic-type fluctuations (Fig. 4b) while, for short-term fluctuations, $Q_{drop} = 0.67$ (Fig. 7). We can say that we achieve stable long and short-term variations with the averaged time series of velocity changes from 3 and 20 station pairs (Figs 17 and 18) since the mean coherence level of real CCFs for both cases ($coh = 0.41$) is greater than those in the synthetic averages of inverted time series of velocity changes over different station pairs (Figs 5a and 8a). Considering the uncertainties associated with the measurements, in case of seasonal variations, the correlation with the expected velocity curves of the reconstructed time series of velocity changes goes from 0.22 ± 0.28, in case of one station pair used, to 0.38 ± 0.25, averaging over 3 station pairs, and to 0.74 ± 0.10 with 20 station pairs (Fig. 5a). This means that, in cases of very low *coh*, the correlation increases by a factor between $\dfrac{0.38 - 0.25}{0.22 + 0.28} = 0.3$ and $\dfrac{0.38 + 0.25}{|0.22 - 0.28|} = 10.5$, averaging over 3 station

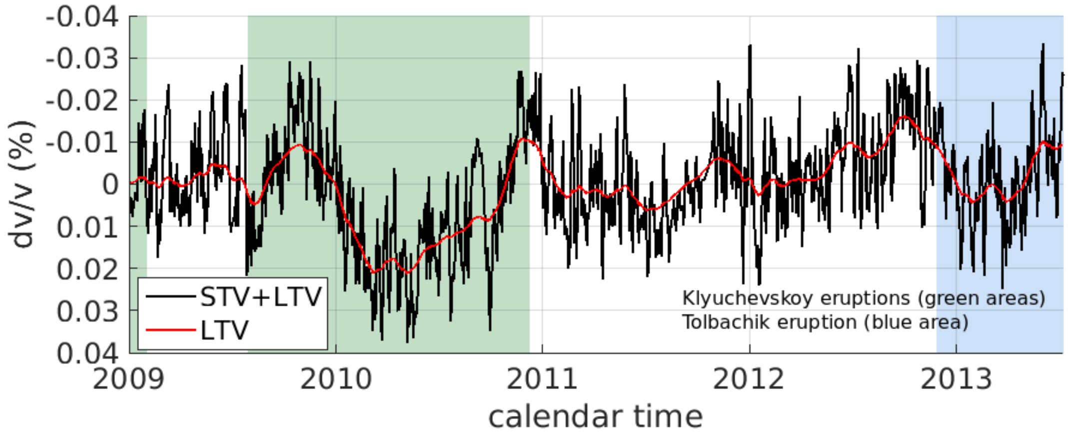

Figure 17. Evolution of relative velocity changes measured from three stations located near Shiveluch from January 2009 to August 2013. Raw relative velocity changes (STV+LTV in black) and long-term velocity variations (red curve) are overlaid. Klyuchevskoy and Tolbachik eruptions are shown with green and blue rectangles, respectively.

pairs, and between $\dfrac{0.74-0.10}{0.22+0.28}=1.3$ and $\dfrac{0.74+0.10}{|0.22-0.28|}=14$ with 20 station pairs. It is important to note that, for long-term and short-term variation, averaging over different pairs keeps these changes underestimated (Figs 5a and 8a) but the SNR increases by a factor of 1.6 when considering 3 station pairs instead of only one, and up to 2.5 with 20 station pairs (Fig. 8a). The increase of the SNR allows a better estimate of the timing of the abrupt velocity changes.

We also improve the ability of our method to recover velocity changes during the occurrence of low-frequency volcanic tremors by averaging different synthetic station pairs (Fig. 11a). Although there are high correlations between CCFs when high tremor activities take place (around 0.8 during 2010 and 2013 periods in Figs 14 and 16), the mean coherence level of the CCFs used in the final inversion is low ($coh = 0.41$). Taking into account our synthetic results, in the situation of strong noise perturbations in the noise-correlation shape, when the correlations are highly unstable and, therefore, the coherence level is low, we need to average over enough station pairs. By averaging over 20 station pairs the correlation of the reconstructed time series of velocity changes with the expected velocity curve increases by a factor between 2.2 and 17.3, in regard to a single station pair (Fig. 11a). However, we would retrieve more proper short to medium-term velocity changes due to episodic volcanic tremors by averaging over more than 40 station pairs, to interpret these velocity drops and retrievals without ambiguity (Fig. 11a).

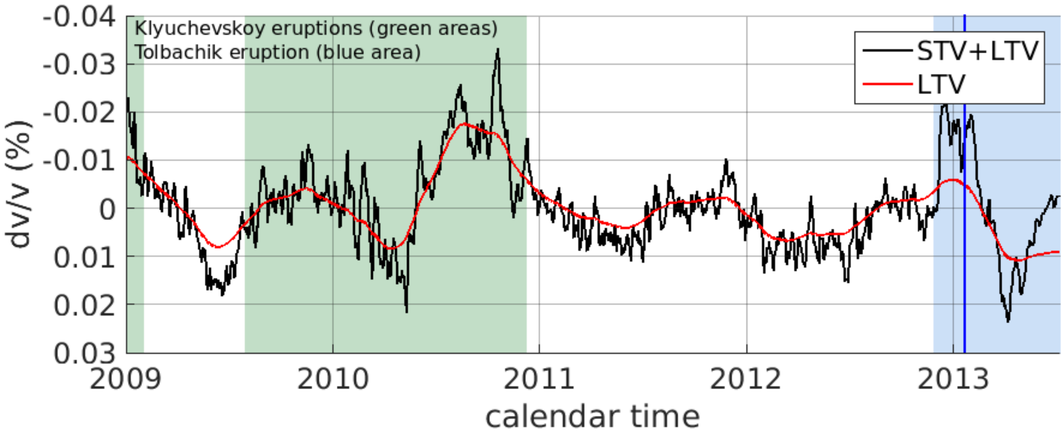

Figure 18. Evolution of relative velocity changes on Klyuchevskoy volcanic group from January 2009 to August 2013 (averaging of time series of velocity changes over 20 station pairs). Raw relative velocity changes (STV+LTV in black) and long-term velocity variations (red curve) are overlaid. Klyuchevskoy and Tolbachik eruptions are shown with green and blue rectangles, respectively.

5 INTERPRETATION OF THE RESULTS

The seismic velocity variations measured near Shiveluch (Fig. 15) are difficult to interpret because this measurement was done only with three station pairs and is, therefore very noisy. Besides, the measurements made with 20 station pairs surrounding the Klyuchevskoy group of volcanoes show velocity variations that can be interpreted in relationship of eruptive history of the two most active volcanoes of this group: Klyuchevskoy and Tolbachik. The whole velocity variations (STV+LTV) are controlled by the combination of two main mechanisms: by the variations of the media mechanical properties caused by the magma motion and pressurization within the volcano plumbing systems and by the environmental effects. These two mechanisms cannot be simply separated as STV and LTV computed during the data analysis because the long-duration eruptions of Klyuchevskoy and Tolbachik have their imprint on both STV and LTV.

The environmental contribution to the seismic velocity variations is expected to be controlled by seasonal changes in temperature, in hydrological loads, and in snow cover. These seasonal effects are particularly strong in Kamchatka and, therefore, we decided to estimate it and to remove from the whole time series, expecting that the remaining velocity variations mainly reflect the dynamics of the volcano plumbing system. To estimate the average long-term seasonal component from the velocity variation time series shown in Fig. 18, we computed median $\frac{d\nu}{\nu}$ values for every Julian day. Then, the obtained one-year periodic function has been smoothed in a 3-month long moving window. The resulted seasonal variations are shown with a thick gray line in Fig. 19a. The seasonality is very clear with a very pronounced velocity increase during winter (between end of December and end of April) and a pronounced velocity decrease during summer (between end of May and end of August).

After removing this seasonal trend, the velocity variations exhibit three significant periods with decrease over 0.01% (Fig 19b). The first of this velocity drops corresponds to the end of the 2008-2009 Klyuchevskoy eruption. The second drop starts at the end of May 2010 and terminates simultaneously with the 2009-2010 Klyuchevskoy eruption. The third velocity decrease starts approximately simultaneously with the 2012-2013 Tolbachik eruption. Therefore, all detected decreases in seismic velocity are observed during eruptions and most likely reflect the inflation-caused dilation of the shallow crustal layers. Nevertheless, the durations of the observed velocity drops do not exactly coincide with the known periods of eruptive activity. A possible explanation for this is that during the long-duration of Kamchatka volcanoes, the state of the plumbing system exhibits significant changes.

The detailed source analysis of co-eruptive tremors by Soubestre et al. (2017) has identified two separate stages of activity during the 2009-2010 Klyuchevskoy eruption. The second stage that started approximately in May 2010 (indicated with vertical dashed line in Fig. 19b) was more intensive with magma likely moving closer to the surface. The observed velocity drop coincides in time with the

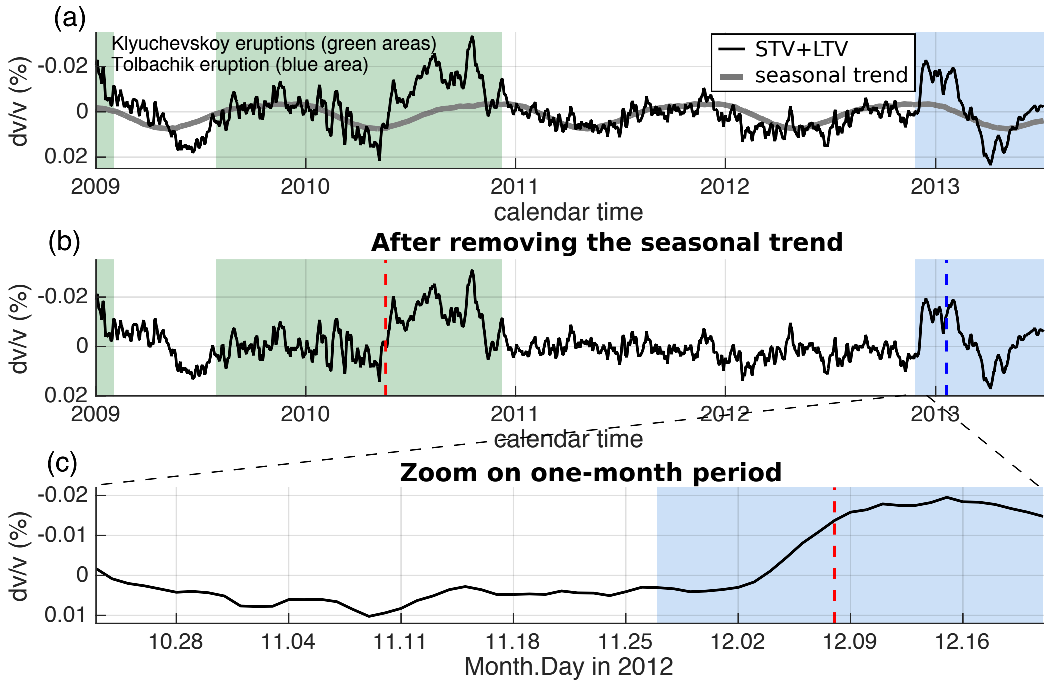

Figure 19. Evolution of relative velocity changes on Klyuchevskoy volcanic group from January 2009 to August 2013 (averaging of time series of velocity changes over 20 station pairs). (a) Raw relative velocity changes (in black) and average seasonal variations (thick gray curve) are overlaid. (b) Velocity variations after removing the seasonal component. Periods of the Klyuchevskoy and Tolbachik eruptions are shown with green rectangles, respectively. The vertical red dashed line indicates the onset of the second stage of the 2009-2010 Klychevskoy eruption (Soubestre et al. 2017). (c) Zoom on one-month period including the beginning of the Tolbachik eruption (green rectangle). The vertical red dashed line indicates the onset of the main eruption stage.

second stage and confirms that the large-scale magma migration occurred between the two stages of eruption.

The level of seismic velocity changes also strongly varied during the 2012-2013 Tolbachik eruption. We observe, in particular, that the onset of the strong velocity drop does not coincide with the beginning of the eruption (Fig. 19c) but rather with the beginning of its main stage when the outpouring of lava concentrated in a single vent where the main eruptive Naboko cone started to grow (Belousov et al. 2015). The later variations in seismic velocities are consistent with changes in tremor sources identified based on correlations of continuous seismic records (Shapiro et al. 2017b).

6 CONCLUSIONS

To summarize, we classify the principal ideas of this work in three itemized sections, according to the methodology, the synthetic tests and the real data results.

- We have proposed a generalized formulation for retrieving continuous time series of velocity changes avoiding the definition of an arbitrary reference CCF.

  - We measure seismic velocity changes between all possible pairs of daily CCFs applying the MWCS analysis.
  - The final time series of velocity changes is obtained by inversion, using a classical Bayesian linear least square formulation. In the inversion, the role of α and β, the regularization parameters, is essential.
  - After inverting, we sort STV and LTV. We retrieve LTV choosing a large β. We further compute STV subtracting the LTV from the raw relative velocity changes, obtained with a small β in the inversion.

- To check the reliability of our method, we computed synthetic tests with the aim of estimating the expected reliability of velocity temporal changes.

  - To recover stable long-term periodic-type velocity variations produced by a seasonal-type trend, we use $\beta = 1000$ and consider different α, choosing lower values for low coh of the CCFs. We check the improvement associated with averaging over different receiver pairs even when the coh between daily cross-correlation functions is quite low.
  - We reconstruct short-term velocity fluctuations (sudden velocity drops) as an effect of a sudden change in the structure, such as an earthquake or a volcanic eruption. We use $\beta = 5$ and $\alpha \approx 0$ in the inversion. Averaging over different station pairs, the sudden velocity changes remains underestimated, however, the SNR of the reconstructed velocity series improves and, therefore, allows a better estimate of the timing of the velocity drop.
  - We also test the ability of our method to retrieve short to medium-term velocity variations (rapid velocity drop and sudden recovery) due to the effect of a transient local source emission, such as a volcanic tremor. We use $\beta = 5$ and $\alpha \approx 0$ in the inversion. Our method produces artificial velocity drops in the situation of strong noise perturbations. In this cases, to retrieve proper velocity changes, we can (1) correct for the artificial baseline difference after inversion if the coherence level between CCFs is high or (2) average over sufficient station pairs when the coherence is low.

- We test and check the suitability and advantage of this approach by applying our method to the

Klyuchevskoy volcanic group dataset of noise cross-correlations, interfered with strong and localized volcanic tremors and the lost of data.

– We compute averaged time series of velocity changes considering, independently, two group of station pairs: 3 station pairs located in the vicinity of the Shiveluch volcano and 20 station pairs, the main group of stations, in the KVG area. The parameters used in the inversion are $\beta = 5$ and $\alpha = 100$ for raw relative velocity changes (STV+LTV) and $\beta = 1000$ and $\alpha = 100$ for LTV.

– For both groups of station pairs (near Shiveluch and the one in the KVG area), the mean coherence level between CCFs is 0.41. The maximum peak-to-peak amplitude of the retrieved LTV and the whole velocity variations (STV+LTV) is about 0.02 %. This allows us to compare with the synthetics. Although short and long-term variations remain underestimated due to edge effects of the time series, we achieve stable long and short-term variations averaging over the main group of station pairs, 20 in total and the SNR increases. Therefore, we have a better estimate of the timing of the abrupt short-term velocity changes. On the other hand, during the occurrence of volcanic tremors we need to average over enough station pairs to ensure there are no artificial baselines, since the coherence level between CCFs obtained from real data is low, 0.41. To interpret velocity drops in these cases without ambiguity, it would be necessary to average over, at least, twice the number of station pairs used (20 receiver pairs).

– STV and LTV cannot be separated in this particular case since long-term eruptions of Klyuchevskoy and Tolbachik are controlled by the fluctuations of the media mechanical properties and by envi-romental effects. After removing the seasonal trend, we observed three velocity decrease periods over 0.01 % related with the inflation-caused dilation of the shallow crustal layers. The first de-crease occurs at the end of the 2008-2009 Klyuchevskoy eruption, the second corresponds to the second stage of the 2009-2010 Klyuchevskoy eruption Soubestre et al. (2017) and the third coin-cides with the beginning of the main stage of the 2012-2013 Tolbachik eruption (Belousov et al. 2015). The duration of these velocity decrease periods does not exactly coincide with the eruptive activity, probably because of the continuous and significant changes of the plumbing system in the Kamchatka volcanoes.

We have established a general framework for this noise-based monitoring technique. Particular care is required to recover temporal velocity variations from CCFs where the noise field recordings are affected by transient tremor signals. In these cases, the processing to monitor active volcanoes is critical. Although, here we use continuous noise-based seismic velocity change observations to provide insights into volcanic unrest, this generalized formulation can be used as well to study crustal earthquake relaxations and the effects of fluid injections in the sub-surface in cases where seismicity interferes with the ambient seismic noise records.

ACKNOWLEDGMENTS

All the data used in this study were provided by the Kamchatka Branch of Geophysical Survey of Russian Academy of Sciences (http://www.emsd.ru). This study was supported by REPSOL CO-DOS project, by the European COST action TIDES (ES1401), by the Russian Science Foundation (grant 14-47-00002), by the French projects 'Labex UnivEarth' and Université Sorbonne Paris Cité project 'VolcanoDynamics' by a research grant from Science Foundation Ireland (SFI) under Grant Number 13/RC/2092 and co-funded under the European Regional Development Fund and by iCRAG industry partners. Computations were performed using the IPGP High-Performance Computing infrastructure S-CAPADE (supported by the Île-de-France region via the SEASAME programme, by France-Grille, and by the CNRS MASTODONS programme).

REFERENCES

Ballmer, S., Wolfe, C. J., Okubo, P. G., Haney, M. M., & Thurber, C. H., 2013. Ambient seismic noise interferometry in Hawai'i reveals long-range observability of volcanic tremor, *Geophysical Journal International*, **194**(1), 512–523.

Belousov, A., Belousova, M., Edwards, B., Volynets, A., & Melnikov, D., 2015. Overview of the precursors and dynamics of the 2012–13 basaltic fissure eruption of Tolbachik Volcano, Kamchatka, Russia, *Journal of Volcanology and Geothermal Research*, **307**, 22–37.

Bensen, G. D., Ritzwoller, M. H., Barmin, M. P., Levshin, a. L., Lin, F., Moschetti, M. P., Shapiro, N. M., & Yang, Y., 2007. Processing seismic ambient noise data to obtain reliable broad-band surface wave dispersion measurements, *Geophysical Journal International*, **169**(3), 1239–1260.

Brenguier, F., Campillo, M., Hadziioannou, C., Shapiro, N., Nadeau, R. M., & Larose, E., 2008a. Postseismic relaxation along the San Andreas fault at Parkfield from continuous seismological observations, *Science*, **321**(5895), 1478–1481.

Brenguier, F., Shapiro, N. M., Campillo, M., Ferrazzini, V., Duputel, Z., Coutant, O., & Nercessian, A., 2008b. Towards forecasting volcanic eruptions using seismic noise, *Nature Geoscience*, **1**(2), 126–130.

Brenguier, F., Campillo, M., Takeda, T., Aoki, Y., Shapiro, N. M., Briand, X., Emoto, K., & Miyake, H., 2014. Mapping pressurized volcanic fluids from induced crustal seismic velocity drops, *Science*, **345**(July), 80–2.

Campillo, M., Sato, H., Shapiro, N. M., & Van Der Hilst, R. D., 2011. New developments on imaging and monitoring with seismic noise, *Comptes Rendus Geoscience*, **343**(8-9), pp–487.

Caudron, C., Taisne, B., Kugaenko, Y., & Saltykov, V., 2015. Magma migration at the onset of the 2012–13 Tolbachik eruption revealed by Seismic Amplitude Ratio Analysis, *Journal of Volcanology and Geothermal Research*, **307**, 60–67.

Chaves, E. J. & Schwartz, S. Y., 2016. Monitoring transient changes within overpressured regions of subduction zones using ambient seismic noise, *Science advances*, **2**(1), e1501289.

Chebrov, V. N., Droznin, D. V., Kugaenko, Y., Levina, V. I., Senyukov, S. L., Sergeev, V. A., Shevchenko, Y., & Yashchuk, V. V., 2013. The system of detailed seismological observations in Kamchatka in 2011, *J. Volcanol. Seismol.*, **7**(1), 16–36.

Chouet, B. A., 1996. Long-period volcano seismicity: its source and use in eruption forecasting, *Nature*, **380**(6572), 309.

Clarke, D., Zaccarelli, L., Shapiro, N. M., & Brenguier, F., 2011. Assessment of resolution and accuracy of the Moving Window Cross Spectral technique for monitoring crustal temporal variations using ambient seismic noise, *Geophysical Journal International*, **186**(2), 867–882.

Colombi, A., Chaput, J., Brenguier, F., Hillers, G., Roux, P., & Campillo, M., 2014. On the temporal stability of the coda of ambient noise correlations, *Comptes Rendus - Geoscience*, **346**(11-12), 307–316.

Dorendorf, F., Wiechert, U., & Wörner, G., 2000. Hydrated sub-arc mantle: a source for the Kluchevskoy volcano, Kamchatka/Russia, *Earth Planet. Sci. Lett.*, **175**(1), 69–86.

Droznin, D. V., Shapiro, N. M., Droznina, S. Y., Senyukov, S. L., Chebrov, V. N., & Gordeev, E. I., 2015. Detecting and locating volcanic tremors on the Klyuchevskoy group of volcanoes (Kamchatka) based on correlations of continuous seismic records, *Geophysical Journal International*, **203**(2), 1001–1010.

Duputel, Z., Ferrazzini, V., Brenguier, F., Shapiro, N., Campillo, M., & Nercessian, A., 2009. Real time monitoring of relative velocity changes using ambient seismic noise at the Piton de la Fournaise volcano (La Réunion) from January 2006 to June 2007, *Journal of Volcanology and Geothermal Research*, **184**(1), 164–173.

Fedotov, S. A., Khrenov, A. P., & Jarinov, N. A., 1987. Klyuchevskoy volcano, its activity in 1932–1986 and possible development, *Volcanol. Seism.*, **4**, 3–16.

Gordeev, E., Murav'ev, Y., Samoilenko, S., Volynets, A., Mel'nikov, D., & Dvigalo, V. N., 2013. The Tolbachik fissure eruption of 2012–2013: Preliminary results, *Dokl. Earth Sci.*, **452**(2), 1046–1050.

Gordeev, E. I., Saltykov, V. A., Sinitsyn, V. I., & Chebrov, V. N., 1990. Temporal and spatial characteristics of volcanic tremor wave fields, *Journal of Volcanology and Geothermal Research*, **40**(1), 89–101.

Hadziioannou, C., Larose, E., Coutant, O., Roux, P., & Campillo, M., 2009. Stability of monitoring weak changes in multiply scattering media with ambient noise correlation: laboratory experiments., *J. Acoust. Soc. Am.*, **125**(6), 3688–3695.

Hillers, G., Husen, S., Obermann, A., Planès, T., Larose, E., & Campillo, M., 2015. Noise-based monitoring and imaging of aseismic transient deformation induced by the 2006 Basel reservoir stimulation, *Geophysics*, **80**(4), KS51–KS68.

Hobiger, M., Wegler, U., Shiomi, K., & Nakahara, H., 2012. Coseismic and postseismic elastic wave velocity variations caused by the 2008 Iwate-Miyagi Nairiku earthquake, Japan, *Journal of Geophysical Research: Solid Earth*, **117**(B9).

Koulakov, I., Gordeev, E. I., Dobretsov, N. L., Vernikovsky, V. A., Senyukov, S., Jakovlev, A., & Jaxybulatov, K., 2013. Rapid changes in magma storage beneath the Klyuchevskoy group of volcanoes inferred from time-dependent seismic tomography, *Journal of Volcanology and Geothermal Research*, **263**, 75–91.

Larose, E., Margerin, L., Derode, A., van Tiggelen, B., Campillo, M., Shapiro, N., Paul, A., Stehly, L., & Tanter, M., 2006. Correlation of random wavefields: An interdisciplinary review, *Geophysics*, **71**(4), SI11–SI21.

Lees, J. M., Symons, N., Chubarova, O., Gorelchik, V., & Ozerov, A., 2013. Tomographic Images of Klyuchevskoy Volcano P-Wave Velocity, in *Volcanism Subduction Kamchatka Reg.*, pp. 293–302.

Levin, V., Shapiro, N., Park, J., & Ritzwoller, M., 2002. Seismic evidence for catastropic slab loss beneath Kamchatka, *Nature*, **418**(6899), 763.

Levin, V., Shapiro, N. M., Park, J., & Ritzwoller, M. H., 2005. Slab portal beneath the western Aleutians, *Geology*, **33**(4), 253–256.

Meier, U., Shapiro, N. M., & Brenguier, F., 2010. Detecting seasonal variations in seismic velocities within Los Angeles basin from correlations of ambient seismic noise, *Geophysical Journal International*, **181**(2), 985–996.

Mordret, A., Jolly, A., Duputel, Z., & Fournier, N., 2010. Monitoring of phreatic eruptions using interferometry on retrieved cross-correlation function from ambient seismic noise: Results from Mt. Ruapehu, New Zealand, *Journal of Volcanology and Geothermal Research*, **191**(1), 46–59.

Nikulin, A., Levin, V., Shuler, A., & West, M., 2010. Anomalous seismic structure beneath the Klyuchevskoy Group, Kamchatka, *Geophysical Research Letters*, **37**(14).

Niu, F., Silver, P. G., Daley, T. M., Cheng, X., & Majer, E. L., 2008. Preseismic velocity changes observed from active source monitoring at the Parkfield SAFOD drill site, *Nature*, **454**(7201), 204.

Obermann, A., Planes, T., Larose, E., & Campillo, M., 2013. Imaging preeruptive and coeruptive structural and mechanical changes of a volcano with ambient seismic noise, *Journal of Geophysical Research: Solid Earth*, **118**(12), 6285–6294.

Ozerov, A. Y., Firstov, P. P., & Gavrilov, V. A., 2013. Periodicities in the Dynamics of Eruptions of Klyuchevskoi Volcano, Kamchatka, in *Volcanism Subduction Kamchatka Reg.*, pp. 283–291.

Poupinet, G., Ellsworth, W. L., & Frechet, J., 1984. Monitoring velocity variations in the crust using earthquake doublets: An application to the Calaveras Fault, California, *Journal of Geophysical Research: Solid Earth*, **89**(B7), 5719.

Rivet, D., Brenguier, F., Clarke, D., Shapiro, N. M., & Peltier, A., 2014. Long-term dynamics of Piton de la Fournaise volcano from 13 years of seismic velocity change measurements and GPS observations, *Journal of Geophysical Research: Solid Earth*, **119**(10), 7654–7666.

Roux, P., Sabra, K. G., Gerstoft, P., Kuperman, W. A., & Fehler, M. C., 2005. P-waves from cross-correlation of seismic noise, *Geophysical Research Letters*, **32**(19), 1–4.

Schaff, D. P., 2012. Placing an upper bound on preseismic velocity changes measured by ambient noise monitoring for the 2004 Mw 6.0 Parkfield earthquake (California), *Bulletin of the Seismological Society of America*, **102**(4), 1400–1416.

Schneider, D., Dean, K., Dehn, J., Miller, T., Kirianov, V. Y., et al., 2000. Monitoring and analyses of volcanic activity using remote sensing data at the Alaska Volcano Observatory: case study for Kamchatka, Russia, December 1997, *Remote Sensing of Active Volcanism*, pp. 65–85.

Sens-Schönfelder, C. & Wegler, U., 2006. Passive image interferemetry and seasonal variations of seismic velocities at Merapi Volcano, Indonesia, *Geophysical Research Letters*, **33**(21), 1–5.

Sens-Schönfelder, C., Pomponi, E., & Peltier, A., 2014. Dynamics of Piton de la Fournaise volcano observed by passive image interferometry with multiple references, *Journal of Volcanology and Geothermal Research*, **276**, 32–45.

Senyukov, S. L., 2013. Monitoring and prediction of volcanic activity in Kamchatka from seismological data: 2000–2010, *J. Volcanol. Seismol.*, **7**(1), 86–97.

Senyukov, S. L., Droznina, S. Y., Nuzhdina, I. N., Garbuzova, V. T., & Kozhevnikova, T. Y., 2009. Studies in the activity of Klyuchevskoi volcano by remote sensing techniques between January 1, 2001 and July 31, 2005, *J. Volcanol. Seismol.*, **3**(3), 191–199.

Shapiro, N. M. & Campillo, M., 2004. Emergence of broadband Rayleigh waves from correlations of the ambient seismic noise, *Geophysical Research Letters*, **31**(7).

Shapiro, N. M., Campillo, M., Stehly, L., & Ritzwoller, M. H., 2005. High-resolution surface-wave tomography from ambient seismic noise, *Science*, **307**(5715), 1615–1618.

Shapiro, N. M., Ritzwoller, M., & Bensen, G., 2006. Source location of the 26 sec microseism from cross-correlations of ambient seismic noise, *Geophysical Research Letters*, **33**(18).

Shapiro, N. M., Droznin, D., Droznina, S. Y., Senyukov, S., Gusev, A., & Gordeev, E., 2017a. Deep and shallow long-period volcanic seismicity linked by fluid-pressure transfer, *Nature Geoscience*, **10**(6), 442–445.

Shapiro, N. M., Droznin, D., Droznina, S. Y., Senyukov, S., Gusev, A., & Gordeev, E., 2017b. Variations of properties of seismic tremor during the 2012-2013 eruption of the Tolbachik volcano based on correlations of continuous seismic records in the Tolbachik fissure eruption of 2012-2013: results of investigations, probability model, role for understanding of basalt eruption in subduction zones, in press (in Russian).

Slavina, L. B., Pivovarova, N. B., & Senyukov, S. L., 2012. Velocity structure of the crust and upper mantle at the northern group of Kamchatka volcanoes (Based on the travel time of P-waves from volcanic earthquakes), *Izv. Atmos. Ocean. Phys.*, **48**(7), 696–705.

Soubestre, J., Shapiro, N., Seydoux, L., de Rosny, D., Droznina, S., Senyukov, S., & Gordeev, E., 2017. Network-based detection and classification of seismo-volcanic tremors: example from the Klyuchevskoy volcanic group in Kamchatka, Manuscript submitted for publication.

Stehly, L., Froment, B., Campillo, M., Liu, Q. Y., & Chen, J. H., 2015. Monitoring seismic wave velocity changes associated with the Mw 7.9 Wenchuan earthquake: increasing the temporal resolution using curvelet filters, *Geophysical Journal International*, **201**(3), 1939–1949.

Tarantola, A., 2005. *Inverse problem theory and methods for model parameter estimation*, SIAM.

Ugalde, A., Villaseñor, A., Gaite, B., Casquero, S., Martí, D., Calahorrano, A., Marzán, I., & Carbonell, R., 2013. Passive seismic monitoring of an experimental CO2 geological storage site in Hontomín, *Seismological Research Letters*, **84**(1), 75–84.

Ugalde, A., Gaite, B., & Villaseñor, A., 2014. Temporal variations of seismic velocity at Paradox Valley, Colorado, using passive image interferometry, *Bulletin of the Seismological Society of America*, **104**(3), 1088–1099.

Wapenaar, K. & Fokkema, J., 2006. Green's function representations for seismic interferometry, *Geophysics*, **71**(4), SI33–SI46.

Wapenaar, K., Draganov, D., Snieder, R., Campman, X., & Verdel, A., 2010. Tutorial on seismic interferometry: Part 1—Basic principles and applications, *Geophysics*, **75**(5), 75A195–75A209.

Wegler, U. & Sens-Schönfelder, C., 2007. Fault zone monitoring with passive image interferometry, *Geophysical Journal International*, **168**(3), 1029–1033.

Yogodzinski, G. M., Lees, J. M., Churikova, T. G., Dorendorf, F., Wöerner, G., & Volynets, O. N., 2001. Geochemical evidence for the melting of subducting oceanic lithosphere at plate edges, *Nature*, **409**(January), 500–504.

Zharinov, N. A. & Demyanchuk, Y. V., 2009. The February – July 2007 Eruption of the Summit Crater of Klyuchevskoi Volcano, Kamchatka, *J. Volcanol. Seismol.*, **3**(3), 179–190.

Zhou, R., Huang, L., Rutledge, J. T., Fehler, M., Daley, T. M., & Majer, E. L., 2010. Coda-wave interferometry analysis of time-lapse VSP data for monitoring geological carbon sequestration, *International Journal of Greenhouse Gas Control*, **4**(4), 679–686.